

Evidence for Middle Palaeolithic occupation and landscape change in central Armenia at the open-air site of Alapars-1

Ariel Malinsky-Buller^{a*} , Phil Glauberman^{b,c,*}, Keith Wilkinson^d, Bo Li^{e,f}, Ellery Frahm^g, Boris Gasparyan^b, Rhys Timms^h, Daniel S. Adlerⁱ, Jennifer Sherriff^{h*}

^aMONREPOS, Archaeological Research Centre and Museum for Human Behavioural Evolution, Schloss Monrepos, D - 56567 Neuwied, Germany

^bInstitute of Archaeology and Ethnography, National Academy of Sciences, Yerevan, Armenia

^cXi'an Jiaotong-Liverpool University, Suzhou, China

^dDepartment of Archaeology, Anthropology and Geography, University of Winchester, Department of Archaeology, Winchester, UK

^eCentre for Archaeological Science, School of Earth, Atmospheric and Life Sciences, University of Wollongong, Wollongong, New South Wales, Australia

^fAustralian Research Council (ARC) Centre of Excellence for Australian Biodiversity and Heritage, University of Wollongong, Wollongong, New South Wales, Australia

^gYale Initiative for the Study of Ancient Pyrotechnology, Department of Anthropology, Yale University, New Haven, Connecticut, USA

^hCentre for Quaternary Research, Department of Geography, Royal Holloway, University of London, Egham, Surrey, UK

ⁱUniversity of Connecticut, Department of Anthropology, Old World Archaeology, Storrs, Connecticut, USA

*Corresponding author at: Schloss Monrepos, D - 56567 Neuwied, Germany. E-mail address: Malinsky@rgzm.de (A. Malinsky-Buller).

(RECEIVED October 3, 2019; ACCEPTED June 16, 2020)

Abstract

Here we report the findings from excavations at the open-air Middle Palaeolithic site of Alapars-1 in central Armenia. Three stratified Palaeolithic artefact assemblages were found within a 6-m-thick alluvial-aeolian sequence, located on the flanks of an obsidian-bearing lava dome. Combined sedimentological and chronological analyses reveal three phases of sedimentation and soil development. During Marine Oxygen Isotope Stages 5–3, the manner of deposition changes from alluvial to aeolian, with a development of soil horizons. Techno-typological analysis and geochemical sourcing of the obsidian artefacts reveal differential discard patterns, source exploitation, and artefact densities within strata, suggesting variability in technological organization during the Middle Palaeolithic. Taken together, these results indicate changes in hominin occupation patterns from ephemeral to more persistent in relation to landscape dynamics during the last interglacial and glacial periods in central Armenia.

Keywords: Middle Palaeolithic; Armenian highland; Palaeolithic; Landscape dynamics; Open-air sites; Republic of Armenia; Hrazdan-Kotayk Plateau

INTRODUCTION

Situated between the Lesser Caucasus Mountains to the north and the Araxes River to the south, the modern Republic of Armenia is characterised by steep elevational gradients (ranging from ca. 400 to 4000 meters above sea level [m asl]) and by ecologically diverse micro-habitats (Volodicheva, 2002). These topographical, ecological, and environmental

conditions provide an ideal location for investigating Palaeolithic settlement patterns, resource use, and technological organisation in the context of environmental fluctuations. Our current knowledge of hominin occupation in the Armenian highlands and the Southern Caucasus during the last 250 ka yr contains many temporal and spatial gaps, with only a few sites attributed to the interglacial periods of marine isotope stages (MIS) 7 to 5 (Pinhasi et al., 2008; Mercier et al., 2010). The majority of chronometrically dated sites fall between ca. 60 and 30 ka BP, during MIS 4 and 3 (Adler et al., 2008, 2012; Gasparyan et al., 2014; Douka and Higham, 2017; Kandel et al., 2017; Glauberman et al., 2020).

Over the last two decades, archaeological research has intensified in the Republic of Armenia, resulting in the discovery and excavation of several Middle Palaeolithic (MP)

*Contributed equally.

We dedicate this paper to the memory of Ofer Bar-Yosef, whose endless curiosity and enthusiasm will continue to guide our research.

Cite this article: Malinsky-Buller, A., Glauberman, P., Wilkinson, K., Li, B., Frahm, E., Gasparyan, B., Timms, R., Adler, D. S., Sherriff, J. 2020. Evidence for Middle Palaeolithic occupation and landscape change in central Armenia at the open-air site of Alapars-1. *Quaternary Research* 1–25. <https://doi.org/10.1017/qua.2020.61>

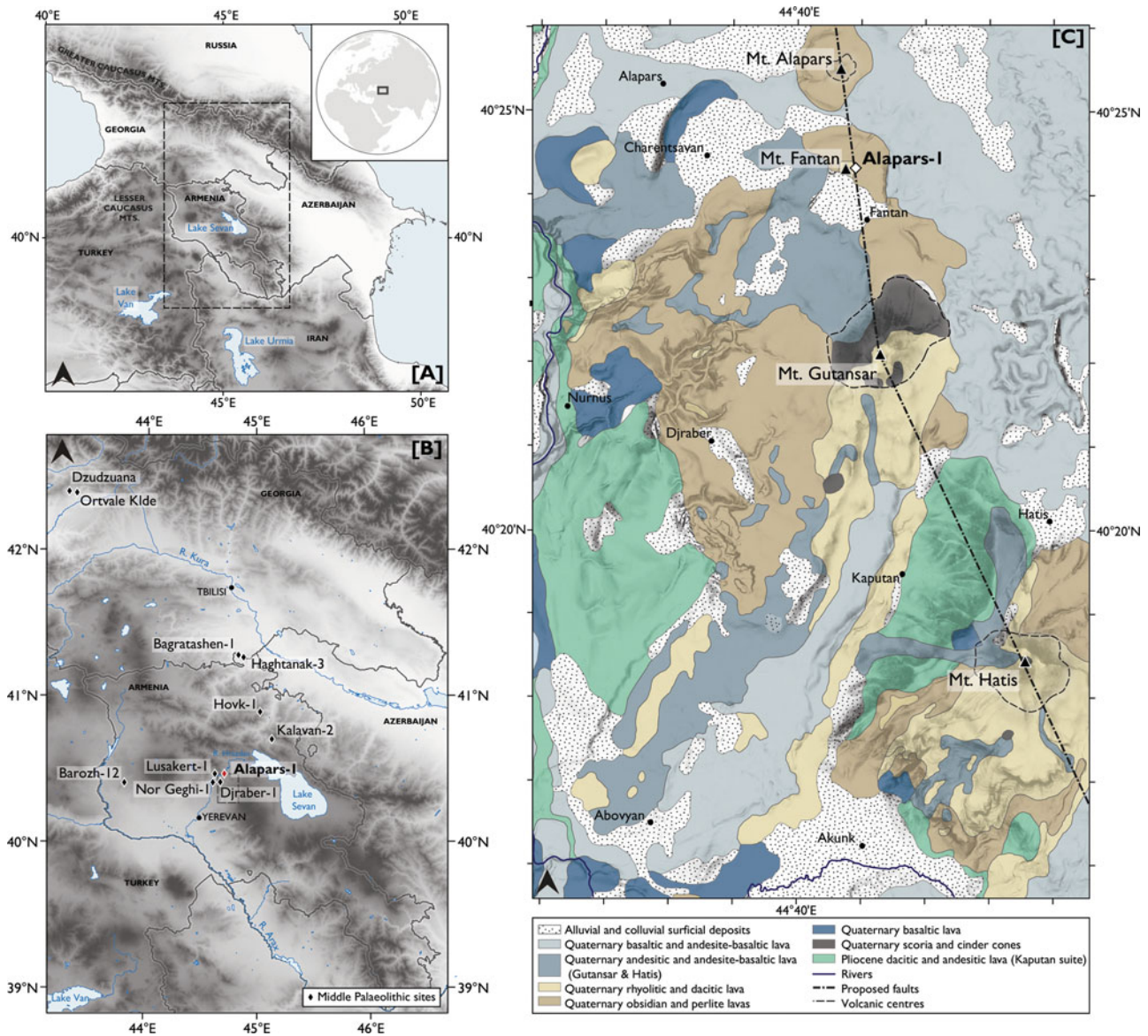


Figure 1. (color online) Location maps showing: (A) the topographical position of the Southern Caucasus; (B) the distribution of known Middle Palaeolithic sites in Armenia and Georgia; and (C) the Quaternary geology of the northwest sector of the Gegham volcanic massif and the Hrazdan River Valley (adapted from Karapetian et al., 2001 and Sherriff et al., 2019).

sites (ca. 300 to ca. 40 ka BP) (Pinhasi et al., 2008; Ghukasyan et al., 2011; Adler et al., 2012, 2014; Bar-Oz et al., 2012; Gasparyan et al., 2014; Glauberman et al., 2016, 2020). Yet despite this progress, current knowledge of the temporal patterns of MP occupations is discontinuous, and without identifying and excavating additional sites, the links between environmental conditions and hominin adaptations cannot be understood.

Here we report our findings from the MP open-air site of Alapars-1 on the Hrazdan-Kotayk Plateau; the latter is part of the Gegham volcanic massif in central Armenia (Fig. 1). This site was discovered in 2011 during survey activities conducted as part of the Hrazdan Gorge Palaeolithic Project, an Armenian-American expedition. The site is situated on the edge of a felsic lava dome (Karapetian et al., 2001; Lebedev

et al., 2011) and is thought to have formed during the middle and late Pleistocene as part of the volcanic activity associated with the Gutansar volcanic complex (GVC; Arutyunyan et al., 2007). Excavations in 2015–2016 revealed a ca. 6-m-thick sequence of alluvial and aeolian sediments containing three stratified soil complexes dated to MIS 5–3.

Results of geoarchaeological analyses presented in this paper provide chronologically controlled evidence for MP occupation at Alapars-1 during the late middle and late Pleistocene. Three stratified lithic assemblages were recovered, each exhibiting differential artefact densities and techno-typological characteristics that, together with obsidian sourcing, suggest variability in technological organisation, mobility, and land-use behaviours. Alapars-1 offers a diachronic perspective on land-use patterns and MP settlement

systems during MIS 5 to 3 in central Armenia in relation to environmental changes.

GEOLOGICAL CONTEXT

Alapars-1 (UTM 38T 472915 m E, 4472694 m N) is situated at 1774 m asl, 1 km north of the village of Fantan and 28 km northeast of Yerevan. The exposed sequence is on the northern flanks of the Fantan (also known as “Fontan”) obsidian-bearing felsic lava dome. It is important to note that the latter is distinct from the Alapars lava dome, which lies 1 km further north (Karapetian et al., 2001) (see Fig. 1C).

The Fantan Dome, as expressed on the current ground surface, measures 100 m in diameter and 20 m in height. The dome is part of a series of volcanic features forming the GVC over an area of approximately 70 km², in the northwest sector of the Gegham volcanic massif (Karapetian et al., 2001; Lebedev et al., 2013; Frahm et al., 2014). The GVC comprises dacitic-rhyolitic and basaltic-andesitic lava flows, obsidian-bearing felsic lava, and pyroclastic deposits and scoria-rich pyroclastic deposits; it extends to the north and west of the Mt. Gutansar stratovolcano, which is located ca. 3 km south of Alapars-1. Both the Fantan and Alapars domes, together with Mt. Gutansar, are thought to lie along a north-south fault that passes through the GVC (Karapetian et al., 2001) (see Fig. 1C). To the south of the GVC lies a

second stratovolcano, Mt. Hatis, which has associated lava flows and obsidian-bearing felsic deposits that extend principally south of the volcanic cone towards Yerevan (Lebedev et al., 2018) (see Fig. 1C).

The timing of volcanic activity in the northwestern sector of the GVC is based principally on K-Ar and fission track (FT) ages of volcanic deposits (see Sherriff et al., 2019 for a full review). These ages indicate that the principal phase of volcanic activity associated with the formation of the GVC was ca. 700–400 ka, with the formation of obsidian at ca. 0.7–0.48 Ma around the flanks of Hatis and ca. 500 ka yr in the GVC (Lebedev et al., 2013, 2018). It is important to note, however, that ambiguities are associated with the chronological evidence from the volcanic deposits (Mitchell and Westaway, 1999; Sherriff et al., 2019). This is best exemplified by the previously published chronological evidence from the Fantan Dome, with K-Ar dates on extruded obsidian yielding an age of 480 ± 25 ka (Lebedev et al., 2011), whereas FT ages from the same obsidian extrusion have yielded ages of 320 ± 20 ka and 300 ± 20 ka (Badalian et al., 2001).

The Alapars-1 archaeological site lies on a plateau formed of intermediate-felsic lava, representing the northern margin of the GVC (Fig. 2). The plateau has been heavily dissected by weathering and erosional processes, with evidence of past fluvial activity indicated by the occurrence of a 1-km-long, S–N-oriented dry valley located 500 m east of the site (see

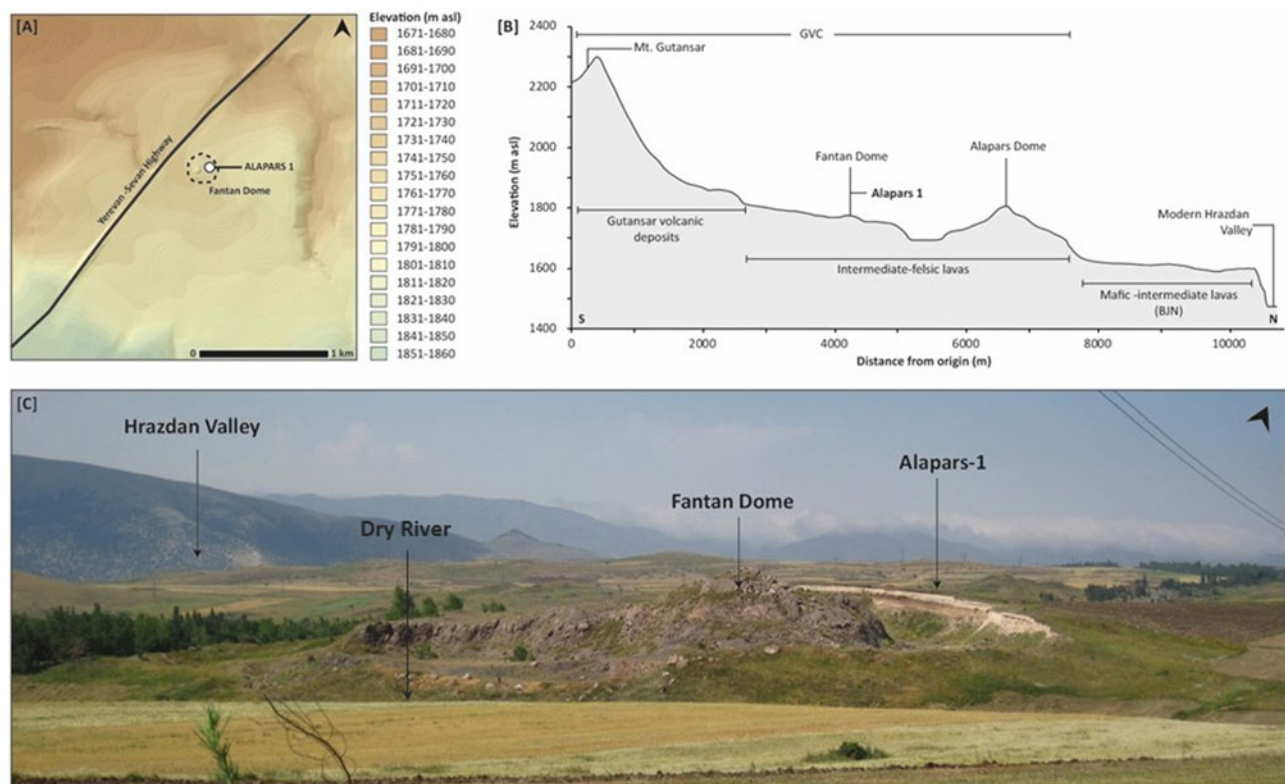


Figure 2. (color online) (A) Topographical map of the Alapars-1 locale; (B) South–north elevational cross-section from Mt. Gutansar to the modern Hrazdan valley. Stratigraphical positions of the main volcanic deposits are labelled, following Sherriff et al. (2019); (C) photograph of the Fantan Dome and Alapars-1.

Fig. 2). A second, lower elevation (1610 m asl) lava plateau lies to the north of Alapars-1, forming the southern margin of the present Hrazdan River valley. Here the Hrazdan River runs E–W and has formed a gorge about 100 m deep, with the present-day channel present at an elevation of 1510 m asl. The river has undergone several phases of geomorphological evolution during the Pleistocene as a response to uplift and volcanic activity. However, based on current chronological evidence, the Hrazdan has been flowing in its current position north of Alapars-1 for about 400 ka yr (Sheriff et al., 2019).

Today, the Hrazdan-Kotayk Plateau is characterised by a continental climate regime, with average summer temperatures of 26°C, average winter temperatures of –13°C, and an average annual rainfall of 500 mm (Volodicheva, 2002). The Pleistocene climatic history of the area is currently poorly understood, with evidence principally based on palaeoecological evidence from Lake Van, Turkey (Litt et al., 2014; Stockhecke et al., 2014; Pickarski et al., 2015a, 2015b; Pickarski and Litt, 2017). This record indicates that warm episodes (interglacials and interstadials) were characterised by Mediterranean-type arboreal vegetation, while non-arboreal taxa associated with cooler and drier conditions characterise cooler stages (glacials and stadials). In recent times, the Fantan Dome has been extensively quarried. As a result, the Alapars-1 sequence is exposed on the northern side of the dome, but the quarrying has removed any physical connection between

the sediments containing the Palaeolithic artefacts and the dome itself (see Fig. 2).

METHODOLOGY

Field and sedimentological methods

A single trench, located in the eastern wall of the quarry, was excavated at Alapars-1 during 2015–2016 (Fig. 3). A total of 21.2 m³ of sediment was excavated, representing (a) an area of ca. 8 m² from 0 cm (zero datum, 1774 m asl) to 120 cm below datum (bd), with a total volume of 9.6 m³, and (b) 4 m² from 120 to 410 cm bd, with a total volume of 11.6 m³. An additional section from 4 m to 6 m bd was cleaned for sedimentological recording. The sediment was excavated in contiguous 10-cm levels and dry-screened through a 5-mm mesh.

Contiguous samples of 5-cm thickness were taken for bulk sedimentological analyses (magnetic susceptibility [χ], percent calcium carbonate, percent total organic carbon [TOC], particle size analysis) through the north profile of Alapars-1 between 50 and 600 cm bd. Samples were oven dried at 40°C, gently disaggregated, and sieved at 2 mm. All analyses were undertaken on the <2-mm size fraction. Mass-specific magnetic susceptibility was measured at low frequency (0.46 kHz, χ^{lf}) and high frequency (4.6 kHz, χ^{hf}) using a Bartington MS2 meter with dual-frequency sensor, following the protocol of Dearing (1999). Values were mass- and

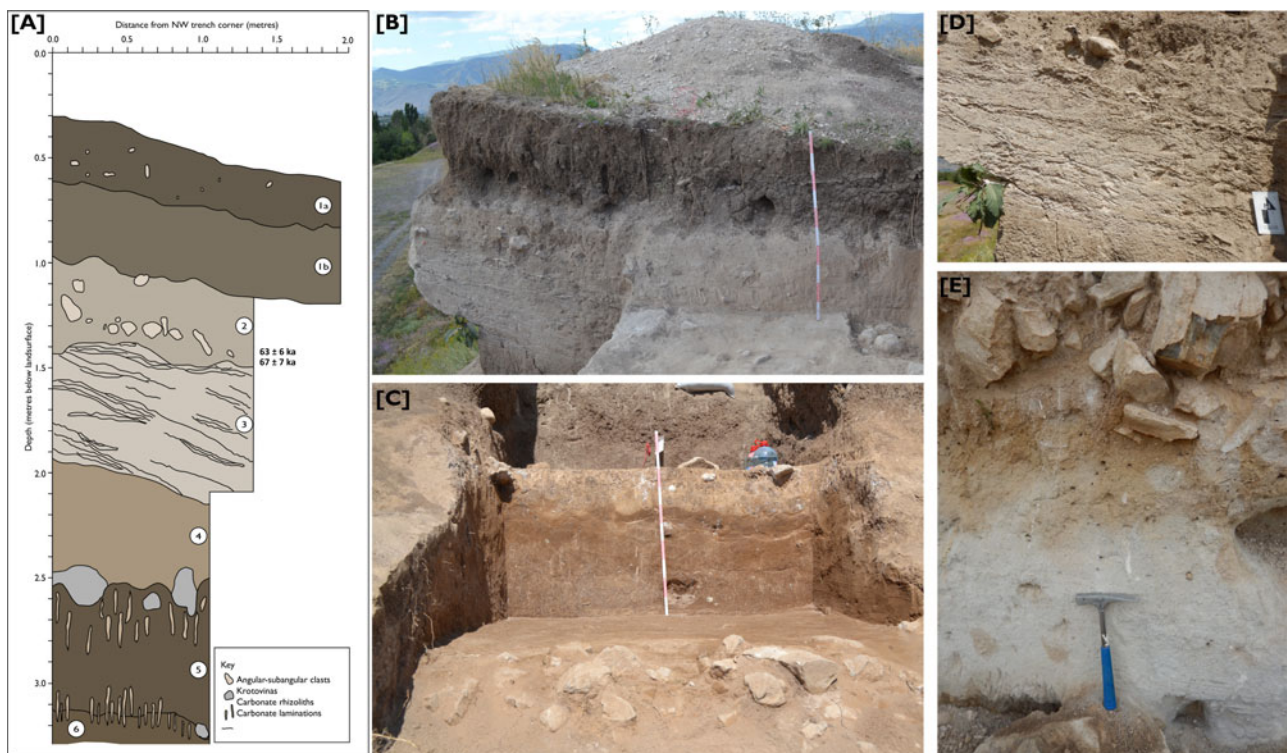


Figure 3. (color online) (A) Section drawing of the upper strata (Units 1–6) of the Alapars-1 sequence. Photographs of the section are shown in b–e, where (B) shows Units 3–1, (C) shows Units 9–4, (D) is a detailed image of Unit 3, and (E) shows Units 12–11.

volume-normalised and are expressed as $10^{-8} \text{ m}^3 \text{ kg}^{-1}$. Percentage frequency-dependent magnetic susceptibility ($\chi^{\text{fd}}\%$) was calculated as: $\chi^{\text{fd}}(\%) = 100 \times [(\chi^{\text{lf}} - \chi^{\text{hf}}) / \chi^{\text{lf}}]$. Calcium carbonate content was measured using a Bascomb calcimeter following the method described by Gale and Hoare (1991), and TOC was measured using the Walkley-Black (1934) titration method. Grain-size analysis was conducted on sand and finer particles by the laser diffraction method using a Malvern Mastersizer 2000 and a Hydro UM accessory. Prior to measurement, calcium carbonate and organic matter were removed through reaction with 10% hydrochloric acid and 10% hydrogen peroxide respectively, and samples were subsequently immersed in 0.5% sodium hexametaphosphate for 24 hours to avoid coagulation. Samples were subjected to ultrasonic cleaning for 20 minutes prior to measurement, and each sample was measured four times using the Mie optical model in 116 channels ranging from 0.004 to 2000 μm . Values presented in Figure 4 represent calculated averages of these individual measurements.

Chronology

Four sediment samples (Table 1), were collected for luminescence dating using opaque stainless-steel tubes hammered horizontally into cleaned stratigraphic sections. Since very little quartz was found in our samples, only potassium-rich

feldspar (K-feldspar) grains were used for dating. Grains with diameters of 90–125 or 90–180 μm were extracted using standard procedures (Aitken, 1998) and measured using infrared stimulated luminescence (IRSL) following the method described in the Supplementary Information. Single aliquots composed of a few hundred grains were measured using an automated Risø thermoluminescence / optically stimulated luminescence (OSL) reader equipped with infrared (875 nm) light-emitted diodes for stimulation (Bøtter-Jensen et al., 2003) and a calibrated $^{90}\text{Sr}/^{90}\text{Y}$ source for beta irradiations. The IRSL emissions were detected using an Electron Tubes Ltd 9235B photomultiplier tube fitted with Schott BG-39 and Corning 7-59 filters to transmit wavelengths of 320–480 nm. IRSL ages from Alapars-1 are presented in Table 1.

In addition to IRSL analysis, contiguous samples of 5-cm thickness from Units 6 to 8 of the Alapars-1 sequence were investigated for their cryptotephra potential, following the methods of Blockley et al. (2005) and Lane et al. (2014). A full description of the protocol and tephra concentrations is presented in the Supplementary Information. Throughout Units 6 to 8, high concentrations of colourless glass shards were identified, with values ranging from 50,000 to ca. 2 million shards g^{-1} dry weight. The distribution profile is, however, continuous and lacks any obvious structure indicative of primary input derived from a volcanic eruption

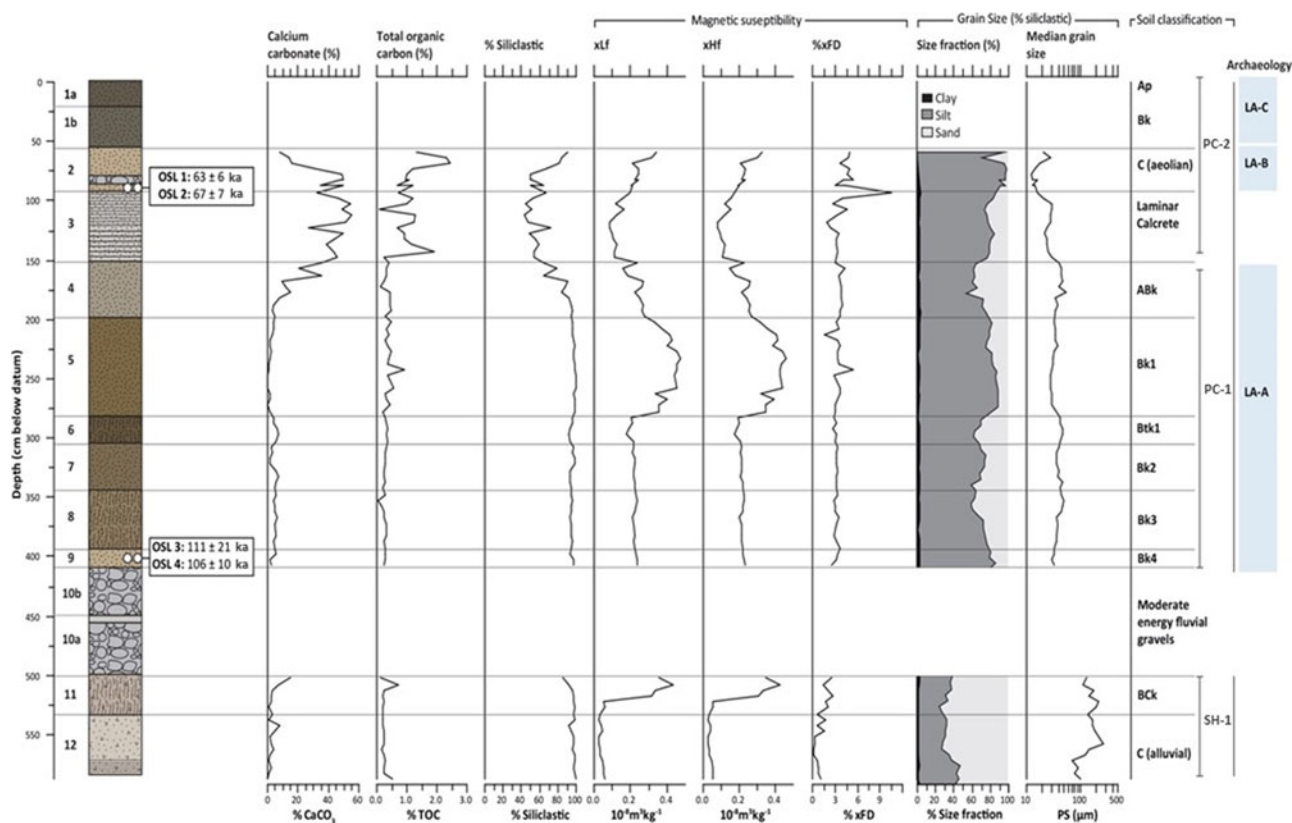


Figure 4. Summary stratigraphical profile of Alapars-1. Shown are the infrared stimulated luminescence age determinations, Unit designations, results of bulk sedimentological analyses (calcium carbonate content, organic content, magnetic susceptibility, grain-size analysis), main pedocomplexes (PC) and Soil Horizons I (SH I), and location of main lithic assemblages (LA).

Table 1. Alapars-1: infrared stimulated luminescence results: burial depths, units, grain sizes, dosimetry data, D_e , and ages for the K-feldspar samples.

Alapars-1 sample	Unit	Depth	Grain size (μm)	Water content (%) ^a	Gamma dose rate (Gy/ka)	Ext. beta dose rate (Gy/ka)	Int. beta dose rate (Gy/ka)	Cosmic ray (Gy/ka)	Total dose		
		below datum in cm							rate (Gy/ka)	pIRIR ₂₉₀ D_e (Gy) ^b	Age (ka) ^b
OSL1	2	90	90–180	15 ± 5 (10)	0.39 ± 0.03	0.62 ± 0.03	0.52 ± 0.09	0.15 ± 0.02	1.68 ± 0.1	115 ± 8	63 ± 6
OSL2	2	90	180–212	15 ± 5 (10)	0.33 ± 0.02	0.49 ± 0.03	0.72 ± 0.13	0.15 ± 0.02	1.49 ± 0.1	123 ± 7	67 ± 7
OSL3	9	400	90–125	15 ± 5 (12)	0.95 ± 0.07	1.44 ± 0.07	0.42 ± 0.07	0.09 ± 0.01	2.91 ± 0.12	332 ± 62	111 ± 21
OSL4	9	400	90–125	15 ± 5 (17)	0.88 ± 0.06	1.39 ± 0.07	0.42 ± 0.07	0.09 ± 0.01	2.78 ± 0.12	305 ± 26	106 ± 10

^aValues used for dose rate and age calculations, with measured (field) water contents shown in parentheses.

^bThe final ages are those obtained from pIRIR₂₉₀ signals. All the ages were calculated by subtracting the residual dose (9 ± 2 Gy) from corresponding D_e values. A relative error of 2% was included in the uncertainty on the final ages, to allow for possible bias in the calibration of the laboratory beta source.

(see Davies, 2015). Therefore, it is likely that the tephra formed a component part of the sediment source material and was not deposited in primary air-fall events (i.e., tephric; see Lowe and Hunt, 2001). Thus, it was decided that the site was not suitable for further cryptotephra-stratigraphical investigation.

Artefact analysis

The lithic assemblages recovered from Alapars-1 were subjected to attribute analysis to assess artefact preservation and were examined for their metrical, technological and, typological characteristics (e.g., Hovers, 2009). The physical properties of the lithic artefacts reflect different natural post-depositional processes. To investigate the taphonomy of artefacts, we analysed edge damage, wear on the ridges of dorsal scars, and patination (Shackley, 1974; Villa and Courtin, 1983; Petraglia and Potts, 1994; Burroni et al., 2002; Anovitz et al., 2006; Glauber and Thorson, 2012, and references therein). The relative sizes and shapes of artefacts, the amount of cortical cover, numbers of dorsal scars, and other characteristics enabled us to reconstruct the core-reduction sequences conducted at the site. Moreover, these attributes allowed us to study the decision-making processes related to the technological organisation and lithic raw material economy of Palaeolithic foragers (Binford, 1979; Geneste, 1985; Kuhn, 1995).

Obsidian artefact sourcing

X-ray fluorescence (XRF) techniques have frequently been used for obsidian sourcing since the 1960s, and portable XRF (pXRF) has become an established tool for such analyses over the last several years (e.g., Frahm and Feinberg, 2015, and references therein). Therefore, given that all lithic artefacts recovered from the site were made of obsidian, a sample ($n = 736$) was geochemically examined using a Niton XL3t 950 GOLDD+ pXRF instrument following procedures described by Frahm (2014). Study of the Alapars-1 artefacts was coupled with pXRF examination of the nearest obsidian sources, including the lava dome on which the site is located.

RESULTS

Alapars-1 site stratigraphy and archaeological context

The Alapars-1 sequence is illustrated in Figure 3, and the bulk sedimentological properties are presented in Figure 4. The sequence comprises angular boulder-sized blocks of intermediate lava (Unit 13) overlain by 12 sedimentary units that primarily represent low- and high-energy alluvial and aeolian sedimentation. Within the sequence, there is evidence for multiple phases of pedogenesis, represented by three stratigraphically distinct soil complexes (Soil Horizon I, Pedocomplexes I–II), and the development of a laminar calcrete horizon. A summary of the sedimentological properties of the Alapars-1 sequence is presented in Table 2.

Units 12–11 (603–510 cm *bd*)

Unit 12 represents the base of the sequence and comprises massive to horizontally bedded coarse ash-lapilli pumice fragments with abundant fine sand and small granules throughout. There is a graded contact with Unit 11, which in turn has a silty-sand texture comprising coarse ash-lapilli pumice with fine–medium sand grains. Unit 11 is also characterised by the prevalence of pedofeatures, including cm-scale blocky peds, Fe/Mn staining throughout, root casts, and associated vertically orientated carbonate rhizoliths. TOC of Unit 11 is low (<0.7% throughout), while CaCO_3 content increases (from 0% to 15%) through the stratum (see Fig. 4). χ^{lf} values are generally low (less than $0.6 \cdot 10^{-8} \text{ m}^3 \text{ kg}^{-1}$); however, the increase in the upper part of the stratum (to $0.35 \cdot 10^{-8} \text{ m}^3 \text{ kg}^{-1}$) likely reflects increases in Fe and Mn (Dearing, 1999).

Units 11 and 12 are interpreted as representing reworked pumice, with horizontal bedding characteristic of subaqueous sedimentation in an alluvial setting. A volcanogenic origin is supported by the consistently high χ^{lf} values (Dearing, 1999), while the increase in χ^{lf} in the upper part of the strata indicates enhancement of the magnetic signal by ferruginous minerals through pedogenic processes. The presence of carbonate rhizoliths in Unit 11 is consistent with the

Table 2. Alapars-1: stratigraphical summary.

Unit	Depth (cm below datum)	Description	Interpretation
1a	0–22	7.5YR/3/2 (dark brown) massive, well-sorted sandy-silt forming granular peds. Dispersed pebble-sized clasts. Sharp contact with:	Soil horizon (Ap)
1b	22–56	10 YR 4/2 (dark greyish-brown) well-sorted humic silt. Strongly developed blocky peds. Vertical cm-scale burrows and rip-up clasts of Unit 2 material associated with lower contact. Millimetre-scale spherical and sub-spherical carbonate nodules present in the lower part of the unit, increase in frequency towards the base. Sharp contact with:	Soil horizon (Bk)
2	56–94	10YR/7/2 (light grey) massive, very well-sorted clay-silt. Modern rhizoliths and isolated granules throughout. Cobble band present at 88 cm. Clasts are heavily weathered, sub-rounded, rhyolitic lithologies. Bed dips downwards towards section face. Diffuse contact with:	Pedogenically modified aeolian deposit (C)
3	94–153	10YR/8/1 (white) indurated fine-grained silt-fine sand with carbonate. Present are 4–8-mm-thick laminations of carbonate (some are heavily cemented, others more friable; laminations generally become thicker towards the top of the unit). Towards top of unit, between lamina are small granule-sized nodules of carbonate and non-carbonate silt-sand-sized grains and pumice lapilli. Laminations dipping 10–15 degrees to northeast. Sharp contact with:	Laminar calcrete
4	153–200	10 YR/6/3 (pale brown) massive, very well-sorted silt with powdery carbonate forming granular to sub-angular blocky peds. Rare carbonate stem casts (cm sized) and burrows, which are principally associated with the Unit 5–4 contact. Burrows contain material from Units 2 and 3 and are carbonate cemented. Sharp contact with:	Soil horizon (ABk)
5	200–282	10 YR/4/4 (dark yellowish-brown) massive, fine sand-clay forming well-developed sub-angular blocky peds. At base of unit, sub-rounded cobbles of rhyolite. Graded contact with:	Soil horizon (Bk1)
6	282–306	10 YR/6/3 (pale brown) massive, silty clay forming columnar aggregates with frequent carbonate rhizoliths. Rare sub-rounded rhyolitic clasts. Diffuse contact with:	Soil horizon (Btk)
7	306–345	10YR/3/3 (brown) massive, fine sand-clay forming sub-angular blocky peds. Common carbonate rhizoliths. Sub-angular obsidian pebbles and rhyolite cobbles (rounded) occur at base of unit. Diffuse contact with:	Soil horizon (Bk2)
8	345–394	10 YR/5/3 (brown) massive, fine sand-clay forming sub-rounded blocky peds bounded by carbonate. Frequent carbonate rhizoliths. Diffuse contact with:	Soil horizon (Bk3)
9	394–410	10 YR/4/3 (dark brown) clay-fine sand forming sub-angular block peds. Carbonate rhizoliths. Sharp contact with:	Soil horizon (Bk4)
10a	410–460	Moderately sorted massive, sub-angular gravels in a matrix of fine sand-silt. Same as 10b; however, gravels generally smaller and slightly less clast rich. Cobbles dipping 20 to 30 degrees. Sharp contact with:	Fluvial gravels
10b	460–510	Normally graded, ca. 3-m-long lenticular bed of clast-supported sub-angular cobbles-boulders. Matrix of fine sand-silt (some pumice material). Clasts predominantly fine-grained mafic-intermediate lava lithologies. Top of gravels characterised by discontinuous bands of heavily cemented and wavy laminated carbonate in matrix rich	Fluvial gravels

(Continued)

Table 2. Continued.

Unit	Depth (cm below datum)	Description	Interpretation
11	510–544	sand-silt. Sharp contact with: 10YR/6/4 (light yellowish-brown) normally graded sand-silt to clay forming granular aggregates. Common carbonate rhizoliths and rootlets.	Soil horizon (Bck)
12	544–603	Diffuse contact with: 2.5Y/8/1 (white) massive, well-sorted to horizontally bedded fine sand-small pumice lapilli and sand-granule-sized clasts.	Weakly pedogenically modified pumice (C)
13		Sharp contact with: Angular boulders of intermediate lava.	

development of a Bk–Bc horizon, and a small increase of clay content in this stratum indicates some clay illuviation may have taken place. These latter properties indicate incipient pedogenesis (designated here as Soil Horizon I) within the fluvially reworked pumice.

Unit 10 (510–410 cm bd)

Unit 10 comprises two beds (Units 10a and 10b) of normally graded moderately sorted clast-rich sub-angular cobbles and boulders that dip 20–30° northeast to southwest in a matrix of fine sand-silt with frequent pumice lapilli. Clasts are principally of fine-grained mafic and indeterminate lithologies. These strata form elongated lenticular beds ca. 3 m in length that appear to taper east and west of the Alapars-1 trench borders. Associated with the 10b–10a contact are fragmented cm-scale beds of wavy laminated carbonate.

The geometry of the strata and sorted nature of the sediments in Units 10a and 10b are consistent with channel features that formed within a high–moderate energy flow regime. The angularity of the clasts and occurrence of solely volcanic lithologies indicate a short transportation history, with material derived from weathering of volcanic deposits in higher elevation areas of the GVC to the south of Alapars-1. Transportation of the material likely occurred in a south to north direction and by alluvial fan or fluvial processes (Mather et al., 2017), while channel formation likely eroded the underlying palaeosol, thereby explaining the truncation of Soil Horizon I. The wavy laminated carbonate associated with Units 10b–10a represents the formation of carbonate crusts on the surface bed load deposits as the consequence of CO₂ degassing and microbial action (Pentecost, 2005; Arenas-Abad et al., 2010). The fragmented nature of these features is a consequence of mechanical breakdown of the crusts by later fluvial activity.

Units 9–4 (410–153 cm bd)

Units 9–4 represent a series of tabular beds ranging in thickness from 16 to 82 cm. Unit 9 is a fine sand-silt forming

granule-sized sub-angular blocky peds; it is characterised by low TOC (less than 0.3%) and CaCO₃ (ca. 2%) contents and by relatively low χ^{lf} (0.24 10⁻⁸ m³ kg⁻¹) values. Unit 8 has similar sedimentological properties; however, it is characterised by a greater abundance of carbonate (see Fig. 4), of which mm-scale sub-vertical carbonate rhizoliths and carbonate coatings of peds are common. This is reflected in the relatively higher CaCO₃ content of Unit 8 (ca. 4.8%) in comparison to Unit 9, while its χ^{lf} (0.24 10⁻⁸ m³ kg⁻¹) and TOC (<0.3%) are similar to the lower unit. Carbonate rhizoliths and carbonate ped coatings are also identifiable in Unit 7; however, rhizolith features here are finer and less abundant than in Unit 8. Unit 7 is composed of fine sand-silt with rare sub-angular obsidian pebbles and rounded cobbles of rhyolite. TOC content (<0.3%), CaCO₃ content (ca. 4%), and χ^{lf} (0.22 10⁻⁸ m³ kg⁻¹) values are comparable to those of Unit 8. Similar sedimentological properties are also identifiable in Unit 6 (TOC <0.4%, CaCO₃ ca. 5%, χ^{lf} 0.20 10⁻⁸ m³ kg⁻¹). Unit 5 is also a fine sand-silt; however, it is characterised by an absence of carbonate pedofeatures. This is reflected in the bulk sedimentological properties of the bed; it has a lower CaCO₃ content (1.6%) than the other strata in Units 9–4, and its TOC (0.4%) and χ^{lf} (0.41 10⁻⁸ m³ kg⁻¹) values are relatively high. Unit 4 is characterised by a sandy-silt texture, forming cm-scale granular aggregates, with powdery carbonate and mm-scale carbonate rhizoliths present throughout. The increase in carbonate through this unit is reflected by higher CaCO₃ values (12.5%), while TOC (0.3%) and χ^{lf} (0.24 10⁻⁸ m³ kg⁻¹) values are similar to Units 6–9. Burrows are found in association with the contact of Units 5 and 4, while the contact between Unit 4 and the overlying Unit 3 is sharp.

The poorly sorted, fine sand-silt texture of Units 9–4 is consistent with sedimentation in an alluvial setting, likely within a low-energy floodplain (Walling et al., 2004). The occurrences of pedofeatures throughout these strata are indicative of the development of a cumulative palaeosol within the alluvial parent material. This is reflected in the relatively high χ^{lf} values throughout the strata, which are consistent with magnetic enhancement associated with pedogenic processes

(Dearing, 1999). Variations in χ^{lf} values through these strata likely indicate varying contributions of diamagnetic calcium carbonate to the magnetic signal; the highest χ^{lf} values are associated with Unit 5, which has the lowest calcium carbonate content in this part of the sequence (Fig. 5). Collectively, Units 9–4 form a composite palaeosol of multiple Bt/Bk horizons (Pedocomplex I). IRSL age estimates from Unit 9 are 111 ± 21 ka (Alapars-OSL3) and 106 ± 10 ka (Alapars-OSL4).

Units 3–2 (153–56 cm bd)

Unit 3 is characterised by carbonate structures with a small fraction of siliciclastic material. Present in the unit is a 4–8-mm-thick horizontal and sub-horizontal laminated micritic calcite. Interspersed between these beds are granule-sized sub-spherical carbonate-coated grains, silt-sized non-carbonate grains, and granule-sized clasts of reworked pumice lapilli. As one moves upwards through the unit an increase in carbonate content is observable, and carbonate beds ranging in thickness from 2–6 mm appear; the beds dip between 5° and 10° to the northeast. These features are represented by high CaCO_3 values throughout the unit, ranging from 35% to 55%. Associated with these high CaCO_3 values is a concomitant decrease in χ^{lf} values to $0.13 \cdot 10^{-8} \text{ m}^3 \text{ kg}^{-1}$ and TOC of 0.9%. There is a sharp boundary between Unit 3 and the overlying Unit 2. Unit 2 consists of massive, well-sorted silt with powdery carbonate dispersed throughout. Within Unit 2 is a continuous band of cobble-sized clasts (88 cm bd); these are sub-rounded and comprise rhyolitic lithologies with carbonate coatings (see Fig. 3B). Associated with Unit 2 is an increase in TOC in comparison with the underlying strata (ca. 1.2%), a decrease in CaCO_3 content

throughout the stratum (from 40% to 15%), and an increase in χ^{lf} values to $0.24 \cdot 10^{-8} \text{ m}^3 \text{ kg}^{-1}$.

On the basis of our field observations, we have interpreted Unit 3 as microbially influenced calcrete (Knox, 1977; Goudie, 1983; Wright, 1989; Genise et al., 2013), representing the terrestrial accumulation of calcium carbonate in the vadose zone, most likely in a semi-arid climatic regime (Wright, 2007; Alonso-Zarza and Wright, 2010). An aeolian origin of the non-carbonate fraction is suggested by the grain-size distribution of this stratum, which exhibits a shift to a finer texture (see Fig. 5) in comparison to underlying strata (Fedoroff et al., 1994; Alonso-Zarza and Silva, 2002; Meléndez et al., 2011; Huerta et al., 2015). The well-sorted nature and medium-fine silt texture of Unit 2 (see Fig. 5) is also consistent with aeolian source material. Taken together, Units 2 and 3 represent the down-sequence accumulation of calcium carbonate associated with soil-forming processes (Wright, 2007). This is demonstrated through the progressive enrichment of carbonate through Units 2 and 3 and the development of laminar calcrete within Unit 3, indicating pedogenic modification of aeolian parent material. The occurrence of sub-rounded cobble-sized clasts within Unit 2 represents a gravel lag, likely formed by deposition via fluvial processes, potentially a high flow event, followed by deflation of fine-grained material. We interpret Unit 2 as reworked rather than primary aeolian deposits, reflecting the combination of sub-aerial and sub-aqueous weathering and then erosive processes that have acted upon them. Together, Units 3 and 2 represent a compound Bk horizon as part of Pedocomplex II. IRSL age estimates for the two upper samples from Unit 2 are 63 ± 6 ka (Alapars-OSL1) and 67 ± 7 ka (Alapars-OSL2) (see Table 1).

Unit 1 (56–0 cm bd)

The uppermost strata of the Alapars-1 sequence are represented by Units 1b and 1a. Unit 1b has a sharp lower contact with Unit 2, characterised by the presence of vertical and sub-vertical cm-scale burrows and isolated clasts of pumice lapilli. Unit 1b comprises well-sorted silt with cm-scale blocky peds and frequent carbonate rhizoliths. At the top of the sequence, Unit 1a comprises well-sorted humic silt-clay with dispersed sub-rounded pebbles. The current land surface was affected by ploughing. These units are interpreted as Bk and Ap horizons, respectively.

Archaeological stratigraphy and lithic analysis

Lithic analysis

The lithic artefacts were recovered from three distinct positions within the depositional sequence at Alapars-1: Lithic Assemblage A (Units 9–4), Lithic Assemblage B (Unit 2), and Lithic Assemblage C (Units 1a and 1b). Only lithic artefacts were retrieved; faunal remains, if once present, were not preserved. All three assemblages share common MP characteristics, principally Levallois reduction sequences, and no diagnostic artefacts indicative of previous or later periods

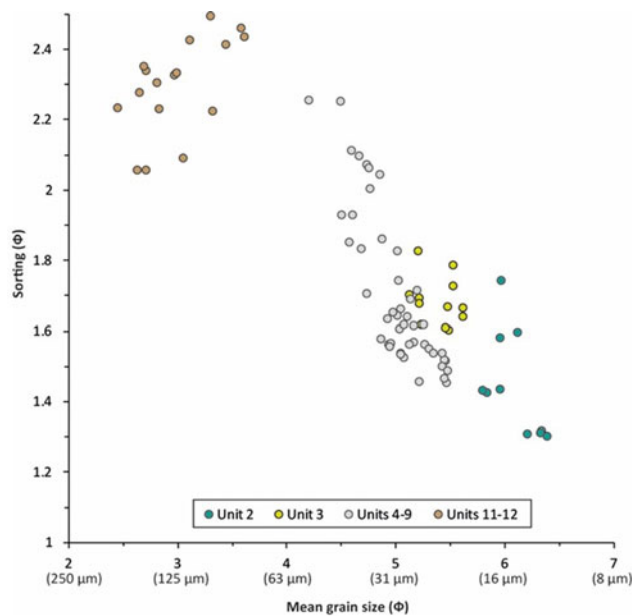


Figure 5. Bivariate plot comparing mean grain size and sorting of Alapars-1 sediments. Mean grain size and sorting are presented on the phi scale and have been calculated following the measures described by Folk and Ward 1957.

have been identified. The three assemblages vary in density of artefacts per m³, preservation and size of the artefacts, and the relative frequencies of the main techno-typological traits (Table 3).

Lithic Assemblage A is dispersed vertically at a very low density over a depth range of ca. 260 cm, yet 75% of artefacts >2 cm (n = 128) and 69% of artefacts <2 cm (n = 254) were recovered from a ca. 60-cm vertical spread in Units 5 and 6 (Fig. 6). This concentration of artefacts is at a low density of 57 artefacts per m³. However, the density of artefacts per m³ in the rest of this sequence is lower still at eight artefacts per m³ (see Fig. 6, Table 3; n = 540, 171 ≥2 cm). Importantly, the concentration appears in two different depositional units within a cumulative palaeosols (Units 5 and 6), thus reflecting deposition over a prolonged period of accumulation.

Lithic Assemblage A (n = 471, 285 ≥2 cm) is primarily composed of well-preserved small non-Levallois flakes (30.6% of the assemblage; Fig. 7A, is an exceptionally large flake). Levallois by-products appear in low frequencies (2.1% of the assemblage), mainly as flake blanks. A low frequency of Kombewa flakes (n = 10, 1.9%) was also observed. Such flakes are commonly by-products of core-on-flake reduction. Four blades were found, comprising 0.7% of the total assemblage (see Fig. 7A–B). One of the blades derives from a Levallois reduction sequence (*sensu* Boëda, 1995; Delagnes, 2000) (see Fig. 7C). Concomitant with a Levallois approach, a ridge blade stemming from a laminar production was found (see Fig. 7B). This ridge blade is a result of rejuvenation of a core from its narrow side. Such a mode of rejuvenation is typical for laminar production (e.g., Meignen, 1998; Delagnes, 2000) (see Fig. 7B). Two bladelets (0.4%) were also recovered (defined as length ≤50 mm, width ≤12 mm; see Bar-Yosef, 1981). The blades and bladelets vary

in size. Diverse modes of production are represented, of which only partial technological stages are represented on-site. The variation in size, the diversity in methods of manufacture, and the fragmentation of the reduction sequence all suggest that blades were produced off site and then transported to this locale.

The average maximum length of the debitage is 30 ± 13 mm (n = 155), with a maximum width of 19 ± 8 mm (n = 155) and a maximum thickness of 6 ± 3 mm (n = 155). The few retouched pieces (n = 7) are larger than the debitage, with an average of 46 ± 14 mm in maximum length, 31 ± 11 mm in maximum width, and 9 ± 4 mm in maximum thickness.

Lithic Assemblage B (n = 471, 285 ≥2 cm, 196 artefacts per m³) is associated with the carbonate-rich, pedogenically modified aeolian parent material of Unit 2. This assemblage is principally composed of both non-Levallois flakes and Levallois flakes and blades, with low frequencies of retouched blanks and cores (see Table 3). Assemblage B also includes cores and core trimming elements (CTEs), suggesting the initial stages of reduction (Fig. 8A–D, see Table 3). Three main core-reduction sequences can be identified: recurrent uni-polar-convergent Levallois flaking (see Fig. 8A–B), core-on-flake reduction (see Fig. 8C–D), and a low frequency of the end-products of blade production (n = 10, 2.1%, see Fig. 9A). Five Levallois uni-polar-convergent cores comprise 27.8% of the cores in Assemblage B. Among the debitage, Levallois blanks and CTEs appear at low frequencies (n = 10, 2.1% of Assemblage B, see Table 3). The Levallois CTEs mainly preserve lateral core curvatures (i.e., *déborderant*, Fig. 9B), with only two overshot flakes. Cores-on-flakes are the most common core category in Assemblage B (n = 10, 55.6% of cores, see Fig. 8C–D). The average maximum

Table 3. Alapars-1: technological breakdown.

Alapars-1	Lithic Assemblage C (Units 1b–1a) (8 m ²)		Lithic Assemblage B (Unit 2) (8 m ²)		Lithic Assemblage A (Units 4–9) (4 m ²)	
	No.	%	No.	%	No.	%
Core	70	5.0	18	3.8	3	0.6
Primary element	1	0.1	15	3.2	7	1.3
Flake	463	33.1	144	30.6	116	21.5
Kombewa flake	-	-	14	3.0	10	1.9
Possible Levallois flake	-	-	4	0.8	5	0.9
Levallois flake	8	0.6	10	2.1	2	0.4
Levallois blade	-	-	-	-	1	0.2
Naturally backed knife	-	-	2	0.4	1	0.2
Core trimming element	33	2.4	15	3.2	7	1.3
Burin spall	-	-	1	0.2	1	0.2
Blade	19	1.4	10	2.1	4	0.7
Bladelet	1	0.1	1	0.2	2	0.4
Tool	51	3.6	43	9.1	7	1.3
Chunk	116	8.3	8	1.7	5	0.9
Flakes smaller than 2 cm	637	45.5	186	39.5	369	68.3
Total	1399	100	471	100	540	100

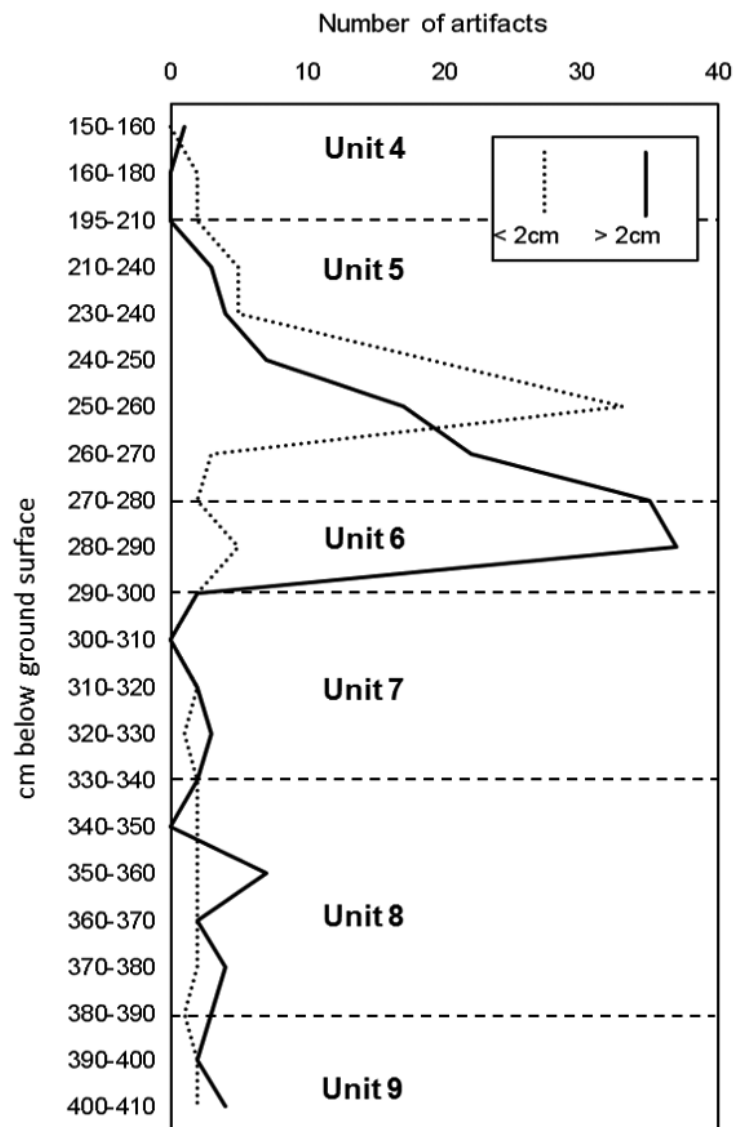


Figure 6. Vertical distribution of lithic Assemblage A within Units 9–4.

dimensions of cores-on-flakes are 53 ± 16 mm in length ($n = 10$), 43 ± 13 mm in width ($n = 10$), and 17 ± 7 mm in thickness ($n = 10$). Comparison with average debitage dimensions (40 ± 18 mm for maximum length, 27 ± 11 mm maximum width, and 11 ± 6 mm maximum thickness, $n = 225$) suggests a deliberate selection of wider and thicker blanks for use as cores-on-flakes. Two-tailed t -tests indicate that cores-on-flakes are significantly wider and thicker than the debitage (width: $t = 3.35$, degrees of freedom (df) = 275, $P < 0.05$; thickness: $t = 2.53$, $df = 276$, $P = 0.03$). Cores-on-flakes vary in their mode of preparation: some lack preparation of a striking platform prior to the removal of secondary blanks (see Fig. 8C), while, in a few instances, truncation was used as a preparatory stage prior to the secondary removal of flakes (following Schroöder, 1969 or Solecki and Solecki, 1970) (see Fig. 8D).

Lithic Assemblage C ($n = 1399$, $762 \geq 2$ cm, 350 artefacts per m^3) is composed largely of non-Levallois flakes ($n = 463$,

33.1%) to a considerable degree. Levallois flakes ($n = 8$, 0.6%), CTEs ($n = 33$, 2.4%), a few tools ($n = 51$, 3.6%), and cores ($n = 70$, 5%) occur at lower frequencies (see Table 3). Only MP artefacts were recovered. This assemblage was recovered from the upper soil horizons of Pedocomplex II which, as discussed above, likely represents a modification of the most recent land surface by ploughing. Consequently, the assemblage was classed as being in a secondary context and no attribute analysis was performed.

In all analysed assemblages, the frequency of breakage among pieces > 2 cm in maximum dimension is relatively high, at 85% in Assemblage B and 90% in Assemblage A. Yet, the preservation of the scars and edges in Assemblage A differs greatly from Assemblages B and C (see Burrioni et al., 2002 for definitions of the terms used). In Assemblage A, 88.3% of the debitage pieces are fresh, while in Assemblage B only 49.3% are fresh, with 41.8% slightly abraded and 8.9% heavily abraded. A similar differential pattern

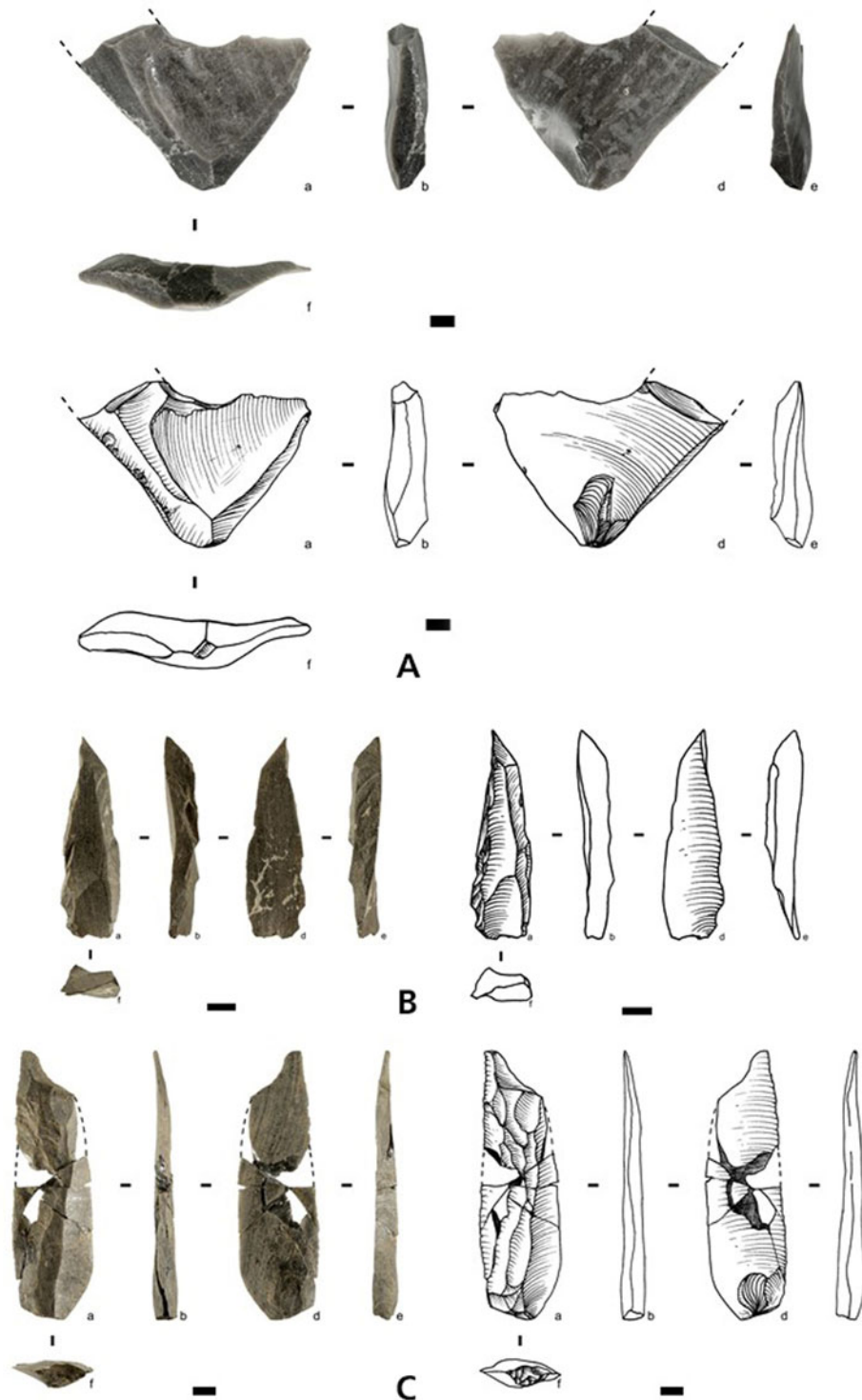


Figure 7. (color online) (A) Broken flake (Assemblage A); (B) ridge blade (Assemblage A); (C) Levallois blade (Assemblage A).

occurs regarding artefact weathering, with patinated items in Assemblage A amounting to only 11.0% of the artefacts, while in Assemblage B 42.7% of the debitage is patinated. Abrasion of artefacts suggests their movement in water and/or sediments (Burroni et al., 2002).

Another indicator of the depositional differences between Assemblages A and B is the low number of

artefacts <2 cm in maximum dimension in Assemblage B (39.5%), compared to their abundance in Assemblage A (68.3%, see Table 3). The higher proportion of small artefacts in Assemblage A runs counter to the lack of indications for on-site knapping. In contrast, Assemblage B, with its indications of on-site knapping, displays a much lower relative frequency of the small fraction (see below).

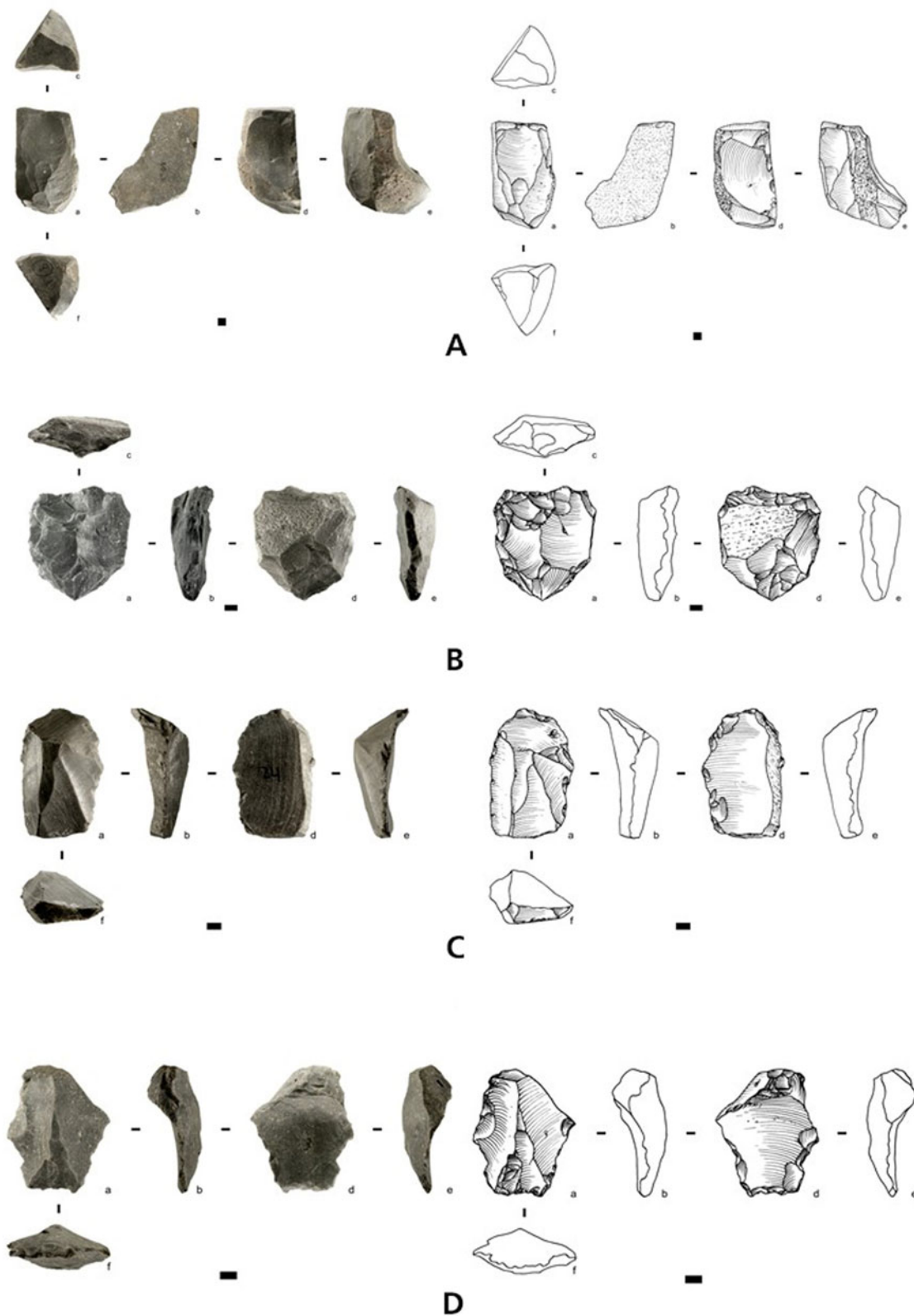


Figure 8. (color online) A-B) Levallois cores (Assemblage B); (C-D) core-on-flake artefacts (Assemblage B).

Based on experimental studies, the expected proportion of artefacts <2 cm in undisturbed assemblages resulting from discrete knapping events ranges between 60% and 85% of all artefacts (Schick, 1986). Such a discrepancy between

the expected proportion of artefacts <2 cm and the proportion found in Assemblage B can be interpreted as the result of post-depositional winnowing of the smaller and lighter artefacts by low-energy water flow. The low frequency of

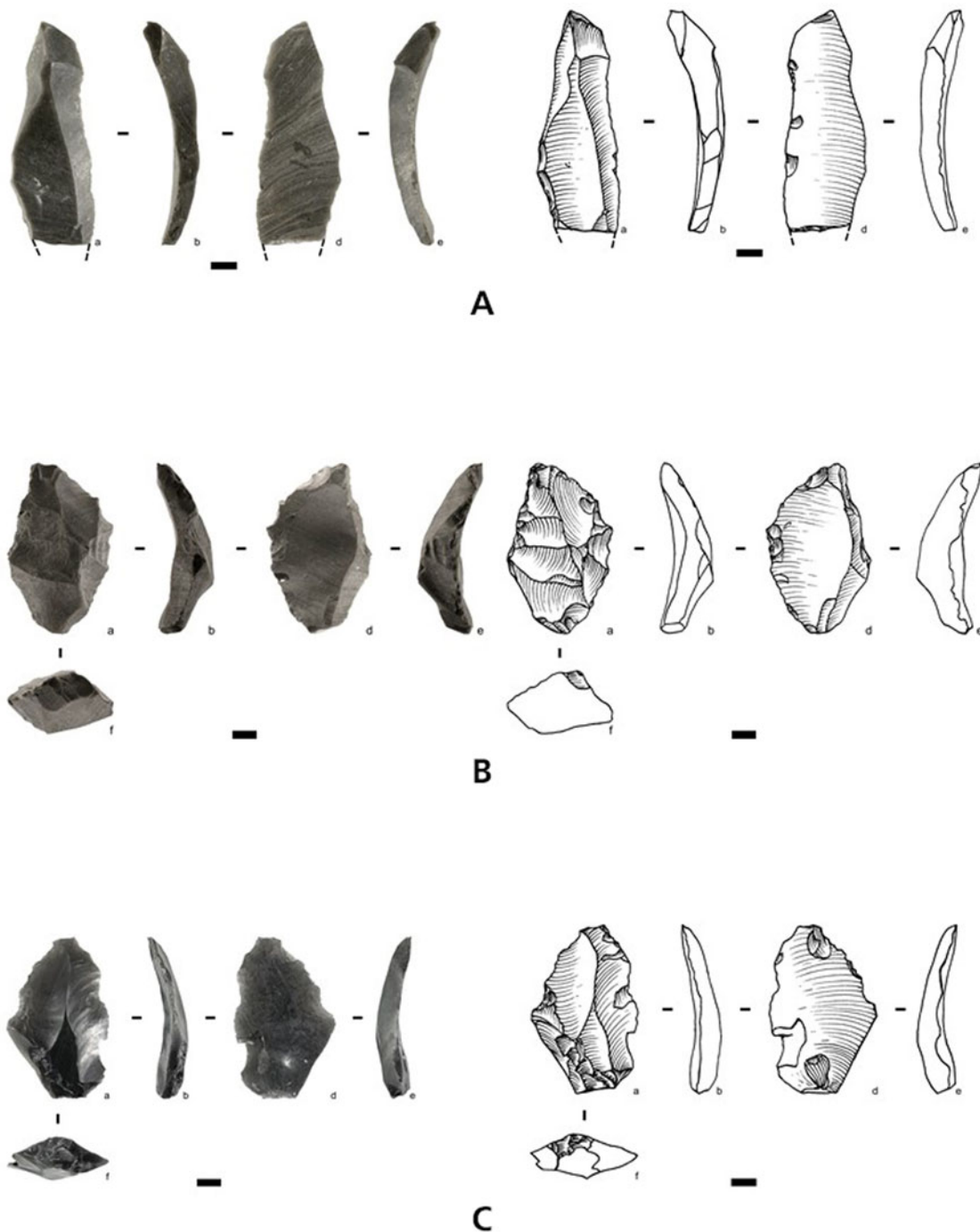


Figure 9. (color online) (A) Blade (Assemblage B); (B) core trimming element-*débordant* (Assemblage B); (C) Levallois flake (Assemblage B).

small artefacts in Assemblage B and the combination of abrasion and weathering features on larger artefacts are likely products of the complex depositional history of Unit 2. The documented phases of deposition, deflation, and post-depositional translocation of material all likely resulted in the recurring exposure of artefacts to atmospheric conditions.

Beyond site formation differences, there are also differences in the relative frequencies of the main technological categories between the Lithic Assemblages A and B (see

Table 3). In Assemblage A, there are fewer indications for on-site knapping: only a small number of cores, low frequencies of primary elements (with cortex covering more than 50% of dorsal surfaces), few CTEs, and no hammerstones were found (see Table 3).

Retouched artefacts in Assemblages A and B share common features related to the selection of blanks. The retouched component in Assemblage B averages 56 ± 27 mm in maximum length, 35 ± 15 mm in maximum width, and 14 ± 6 mm in maximum thickness ($n=43$). The blanks chosen for further

retouch are larger in Assemblages A and B than the debitage (see above) (see Fig. 9). In addition, variation in the relative frequencies of the retouched pieces among the two assemblages is observable, with significantly more retouched blanks in Assemblage B than Assemblage A (9.1% vs. 1.3% respectively; $\chi^2 = 30.62$, $df = 1$, $P < 0.05$; see Table 3).

Classifying edge modifications as intentional retouch in Assemblage B was difficult due to post-depositional forces possibly mimicking retouch. However, despite this confounding factor and our necessarily conservative classification, Assemblage B contains a larger variety of tool types than Assemblage A. These include combination tools (mixtures of scraper retouch, truncation, and notches or isolated removals, e.g., Fig. 10A–B) and other tool types such as scrapers, retouched pieces, and truncations. Assemblage A, on the other hand, contains mainly combination tools (retouched flakes and end-scrapers) and end-scrapers and notches (following Bordes, 1961) (Table 4).

Assemblage B exhibits evidence for nearly all stages of core reduction, including flake production, tool production, and use. The relatively high frequency of retouched artefacts in Assemblage B, many of which exhibit more than one type or location of retouch, suggests longer histories of use and reuse of these items. The comparisons between the technological traits of Assemblages A and B, taking into account differences in artefact density and tool frequencies, suggest a longer duration of occupation and/or more frequent re-occupations during the times of deposition of Assemblage B when compared to the relatively short or infrequent occupations that resulted in Assemblage A.

Obsidian artefact sourcing

Artefacts from all stratigraphic units were analysed using pXRF to determine their elemental compositions and, in turn, volcanic sources ($n = 736$). Figure 11A is a scatter plot of Zr/Rb versus Sr/Rb, showing the obsidian sources that match the analysed artefacts. These source attributions are principally based on ratios between the so-called “mid-Z” elements (i.e., Rb to Nb), which yield reliable values for irregular, small, or weathered obsidian artefacts (see Frahm, 2016, and references therein). Out of 736 artefacts (72.8% of Assemblages A and B), 715 (97.1%) matched sources in the GVC, within which the site is located (see Fig. 11B). Obsidian from deposits other than those local to the GVC was identified only in Assemblage B ($n = 21$, 4.5%). Fourteen of these latter artefacts (3.0% of Assemblage B) match the three obsidian sources in the Tsaghkunyats volcanic area ca. 50 km to the northwest. Of these, a chip and a flake match the Tsaghkunyats-1 source, and a retouched tool and five artefacts were identified from the Tsaghkunyats-2 source. Two cores and four broken flakes match the Tsaghkunyats-3 obsidian source. A further six artefacts (1.3%), including chips and a CTE, were made on obsidian from the Hatis volcano ca. 10 km to the south of the GVC. Of all the analysed artefacts from Assemblage B, just one tool (0.2%) was made on obsidian from Pokr Arteni, located ca. 75 km as the crow flies to the west and >100 km on foot (see Fig. 11B).

DISCUSSION

Model of sediment accumulation and landscape development

The sequence at Alapars-1 has yielded evidence for multiple phases of sediment deposition and landscape stability during the late middle and late Pleistocene. A key feature of the Alapars-1 sequence is the geomorphic association with the Fantan Dome. A K-Ar date, yielding an age of 480 ± 50 ka, has been produced on obsidian that may derive from the dome (Lebedev et al., 2011). Although chronological evidence from the Alapars-1 sequence indicates a younger date for the sediment deposition, stratigraphic evidence indicates that sediments were unlikely to have been deposited after the formation of the dome in its current morphological state. For example, Unit 10 exhibits a dip of $10\text{--}16^\circ$ to the northeast (see Fig. 2, Table 2), which is an unnaturally steep slope for channel or locally derived debris flow deposits given the current geometry of the landscape (see Fig. 2). Furthermore, the formation of the laminar calcrete characterising Unit 3 would have likely occurred in areas of subdued relief. Finally, the absence of colluvial deposits comprising material from the dome within the sequence also strongly suggests that deposition of the sediments in Alapars-1 occurred prior to dome formation, but after the deposition of the obsidian and dacite that compose the upper layers of the dome. On this basis, two scenarios explaining the stratigraphic relationship between the dome and the Alapars-1 sequence can be put forward (Fig. 12).

First, the extrusion of the obsidian and lava occurred prior to the formation of the Alapars-1 sequence, resulting in the formation of a low, shallow-gradient lava dome (Fink, 1983) (see Fig. 12, scenario 1). This was followed by the deposition of the Alapars-1 sediments, during which endogenic dome activity occurred, resulting in the inflation of the dome to its current morphological state. Thus, the K-Ar and FT ages from the Fantan Dome represent the earlier phase of exogenous volcanic activity.

The second scenario is that the Fantan Dome represents a cryptodome (Williams and McBirney, 1979; McPhie et al., 1993; Stewart and McPhie, 2003). In this case, intrusive magmatic activity occurred after the emplacement of the Alapars-1 sediments, resulting in the uplift and tilting of the sediment strata and underlying volcanic deposits. In this scenario, the K-Ar dates represent the age of the volcanic deposits that were uplifted as a consequence of later intrusive activity (see Fig. 12, scenario 2). It is important to note that the obsidian and the perlitic and rhyolitic lavas mapped in the vicinity of the Fantan Dome are part of the GVC. These have been dated to broadly the same time span as the obsidian from the Fantan Dome and are also chemically indistinguishable (Karapetian et al., 2001; Lebedev et al., 2011; Frahm et al., 2014). Whichever scenario is correct, the mechanism of the obsidian emplacement in the Fantan Dome, the mode of the dome's formation, and their relationship with the Alapars-1 sequence cannot be fully elucidated without

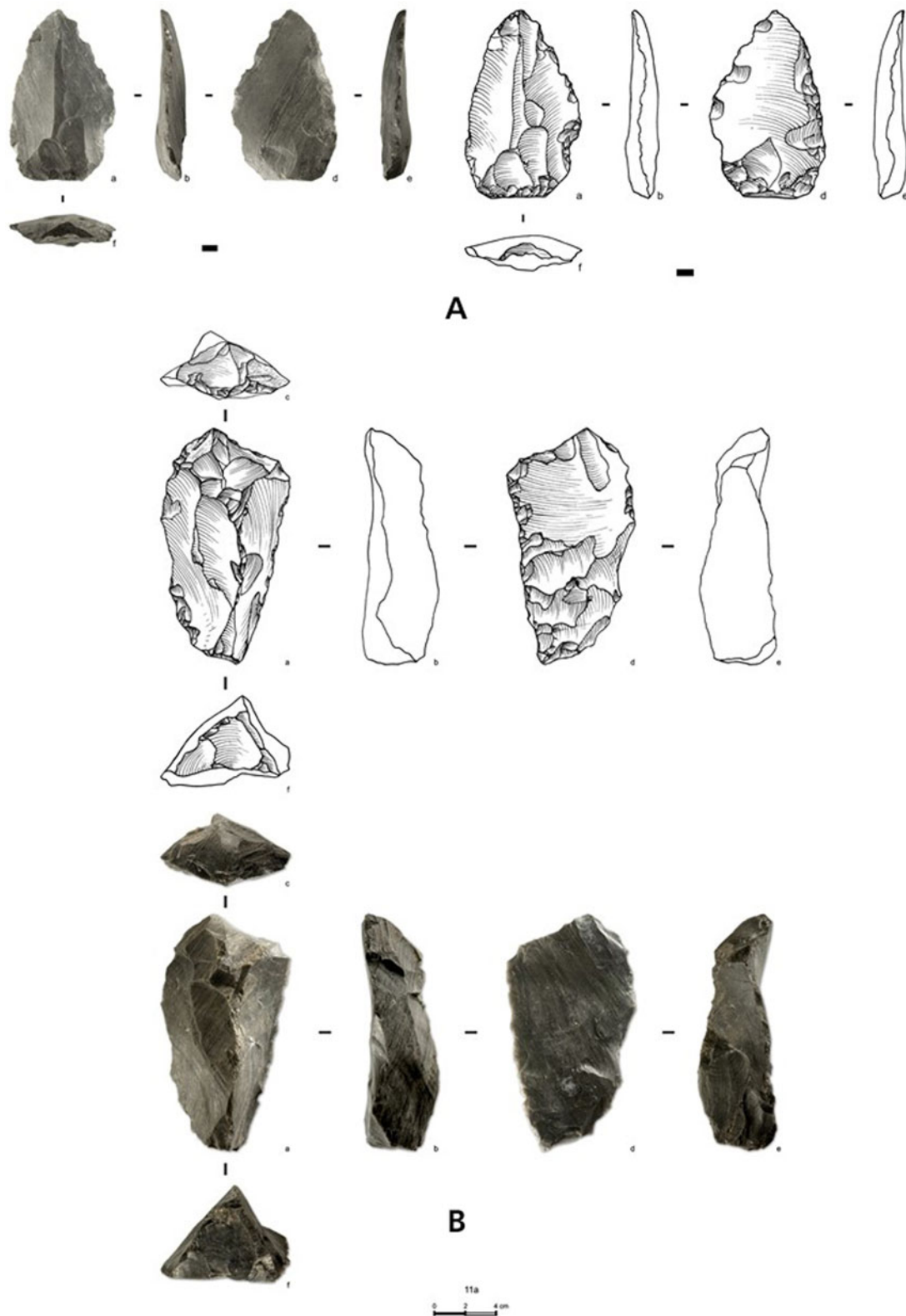


Figure 10. (color online) (A) Combination tool (scraper on ventral face and retouched flake); (B) combination tool (end-scraper and retouched flake); both from Assemblage B.

comprehensive petrological, geochemical, and chronological investigations.

Although detailed micromorphological and geochemical analyses of samples from Alapars-1 are currently ongoing,

the lithostratigraphic evidence reported here provides broad indications of landscape changes occurring in the area during several intervals of the late middle and late Pleistocene. The earliest deposits at Alapars-1, represented by Units 12–9,

Table 4. Alapars-1: typological makeup of retouched tools.

Type	Lithic Assemblage B (Unit 2)		Lithic Assemblage A (Units 4–9)	
	No.	%	No.	%
Combination tool	10	23.3	3	42.9
Single straight scraper	3	7.0	-	-
Single convex scraper	3	7.0	-	-
Double straight scraper	1	2.3	-	-
Side scraper on ventral face	1	2.3	-	-
Typical end-scraper	2	4.7	-	-
Atypical end-scraper	-	-	1	14.7
Atypical burin	1	2.3	-	-
Typical borer	2	4.6	-	-
Truncated flakes and blades	4	9.3	-	-
Awl	1	2.3	-	-
Notch	1	2.3	3	42.9
Retouch on ventral face	2	4.7	-	-
Miscellaneous	1	2.3	-	-
Retouched flake	7	16.3	-	-
Retouched blade	1	2.3	-	-
Isolated removal	3	7.0	-	-
Total	43	100	7	100

indicate several phases of alluvial deposition and pedogenesis subsequent to the emplacement of the lava at the base of the sequence. The onset of fluvial activity at the site is associated with the local reworking of the pumice lapilli deposits, of which several outcrops have been identified in the locality of Alapars-1 (Sherriff et al., 2019). Following this was an

episode of stasis during which the pumice deposits were exposed to sub-aerial weathering, and a soil developed as a result (Soil Horizon I). This was followed by the reestablishment of a fluvial system under a higher-energy flow regime. The bed-form geometry of Units 10a and 10b indicates the stream channel ran in a southeast to northwest direction and likely emanated from the high elevation area around the flanks of the Gutansar volcano. Indeed, the present-day topography of the Alapars-1 locale indicates the occurrence of previous stream activity, with several broadly south to north dry valleys dissecting the lava plateau on which Alapars-1 lies.

Although it was not possible to directly date the deposits of Units 12–10, the IRSL chronology from Unit 9 provides a minimum age estimate, indicating that the lower strata at Alapars-1 were formed prior to 110 ka. Given that, and based on the current chronological evidence from the GVC (namely that the emplacement of volcanogenic deposits in the vicinity of Alapars-1 occurred around 550 ka [MIS 13]), we can hypothesize that the deposition of the Alapars-1 lower strata occurred at some stage during the MIS 12–6 interval.

Units 9–4 mark a shift to lower-energy alluvial sedimentation and accretionary pedogenesis, forming a compound soil profile of several Bt–Bk horizons as a result (Pedocomplex I). Based on the IRSL age estimates of 111 ± 21 ka and 106 ± 10 ka for Unit 9, this shift took place during MIS 5e–5c. Units 9–4 contain the oldest lithic assemblage at the site (Assemblage A). Most artefacts are concentrated at the boundary of Units 6–5, indicating that the earliest occupation of Alapars-1 occurred during MIS 5 (Fig. 13).

The occurrence of several Bt–Bk horizons at Alapars-1 may indicate that conditions were warm and humid during MIS 5. Elsewhere in Armenia, there is evidence for the development of similar soil profiles associated with interglacial warmth (see Wolf et al., 2016; Trigui et al., 2019; Richter

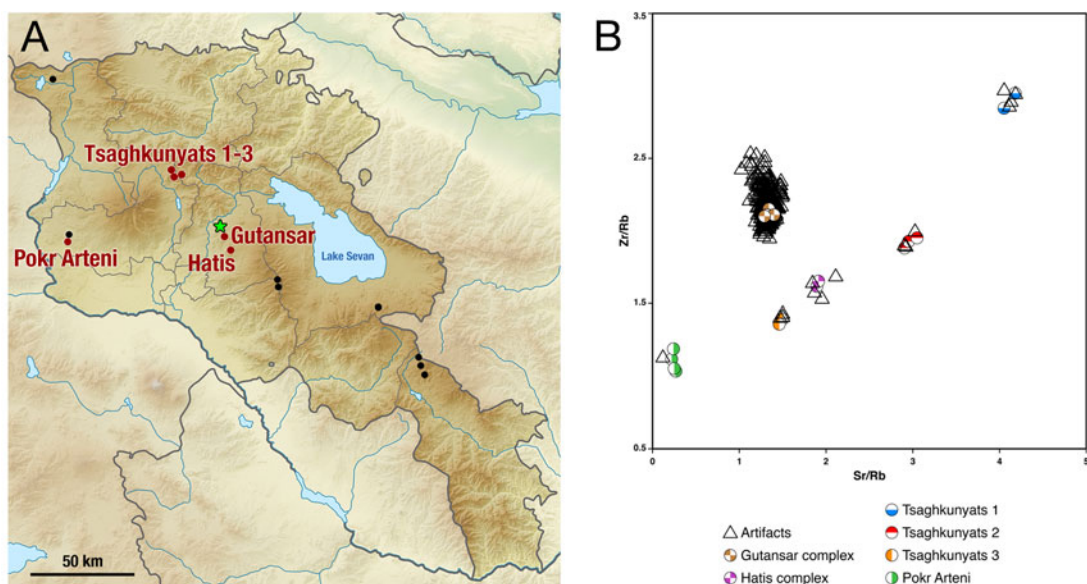
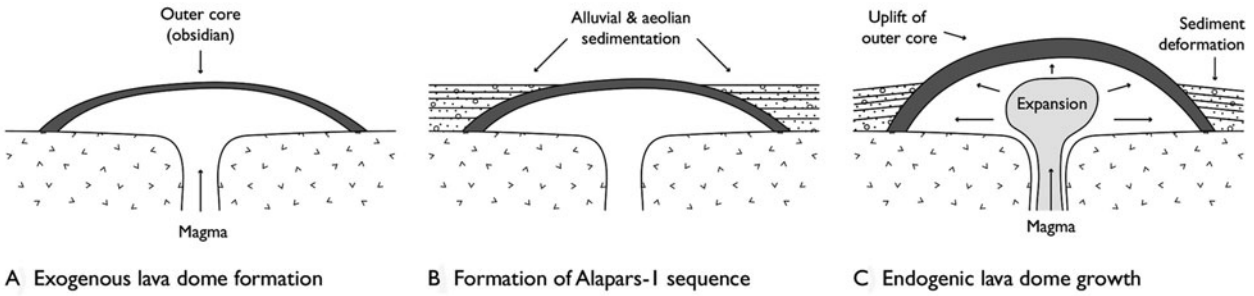


Figure 11. (color online) (A) Scatter plot of Zr and Rb, both normalized to Sr to minimize size effects, for Alapars-1 artefacts and the corresponding geological reference specimens; (A) locations of obsidian sources in relation to Alapars-1.

Scenario 1



Scenario 2

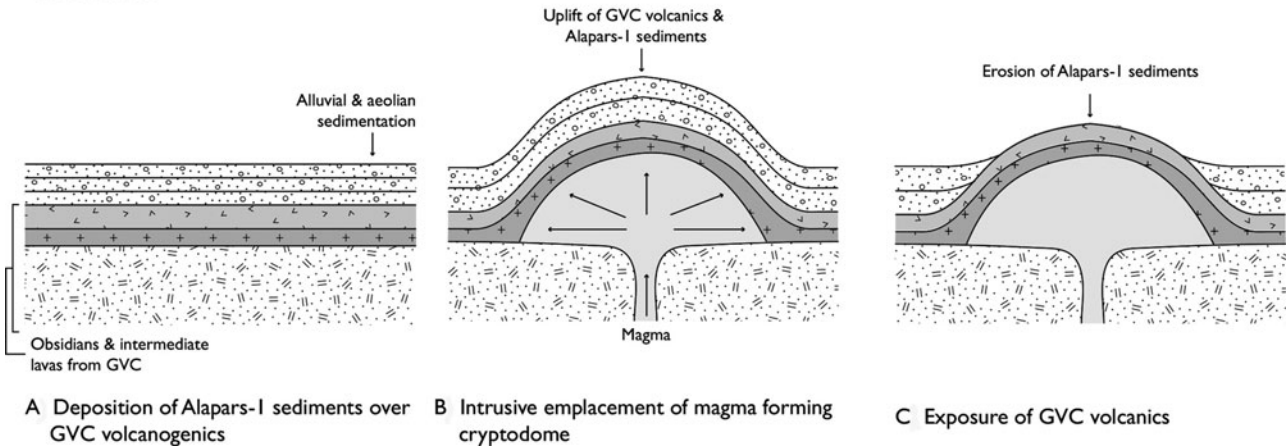


Figure 12. Hypothesised model of dome formation and sedimentation at Alapars-1. Scenario 1 represents exogenous dome growth, sedimentation, and endogenous dome inflation; Scenario 2 represents cryptodome formation resulting in deformation of overlying Alapars-1 sediment strata and volcanic deposits associated with the Gutansar volcanic complex.

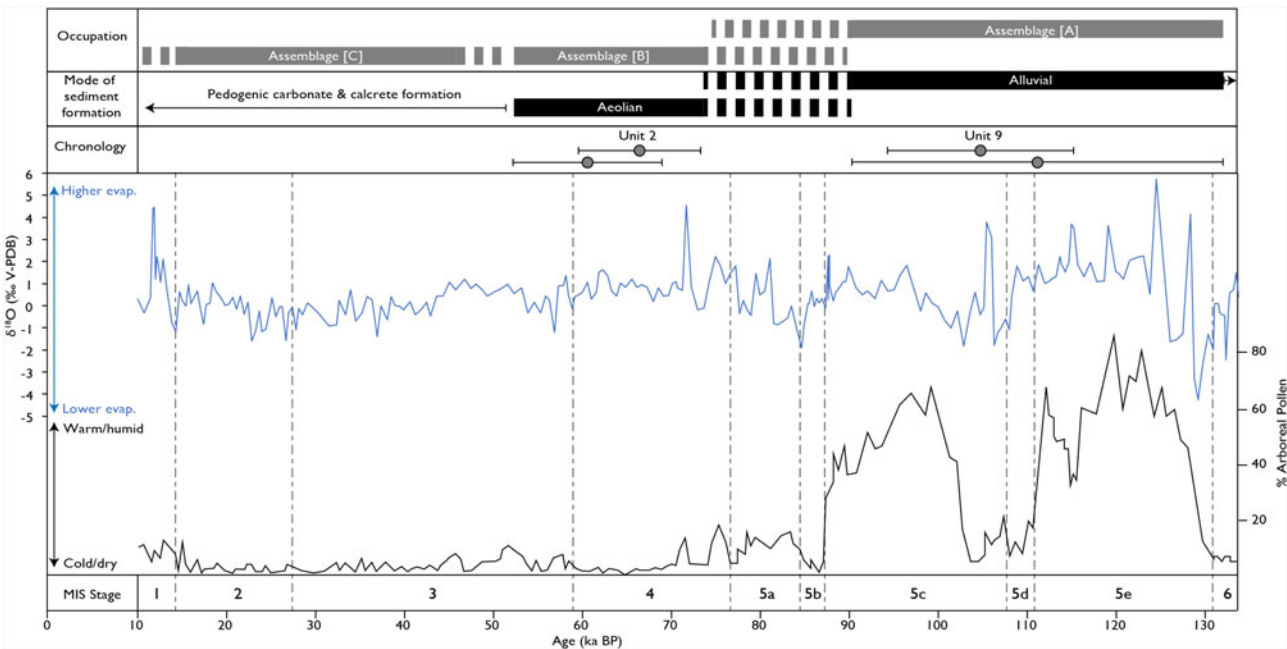


Figure 13. Alapars-1 morphogenic events and occupation levels plotted against Lake Van $\delta^{18}O$ (blue line) and arboreal pollen percentage for the period 10–130 ka BP (Pickarski et al., 2015a, 2015b). (For interpretation of the references to color in this figure legend, the reader is referred to the web version of this article.)

et al., 2020). Although fragmentary in nature, the evidence from these sequences correlates well with palynological evidence from the long lacustrine sequences at Lake Van, Turkey (Litt et al., 2014) and Lake Urmia, Iran (Djamali et al., 2008; Stevens et al., 2012), where warm and humid interglacial periods dominated by the expansion of open deciduous oak steppe-forest are postulated.

A third shift in depositional environment in the Alapars-1 sequence is marked by the onset of aeolian sedimentation associated with Unit 3. While it was not possible to date Unit 3, the IRSL chronology of Unit 2 suggests that the shift to aeolian deposition and sustained periods of arid conditions had already occurred prior to 63 ± 6 ka and 67 ± 7 ka (MIS 4), possibly during the later substages of MIS 5 or early MIS 4. The combined palynological, n-alkane, and geochemical evidence from Lake Van indicates that late MIS 5 and MIS 4 were characterised by dry conditions, punctuated with intervals of warm and wetter conditions (Pickarski et al., 2015a, 2015b; Randlett et al., 2017).

The shift to aeolian deposition in Unit 3 must have been followed by pedogenesis, and therefore stability, given the development of pedogenic carbonates as manifested by field evidence and high CaCO_3e concentrations. The presence of a well-developed laminar calcrete within the Alapars-1 sequence indicates formation under semi-arid conditions (Candy et al., 2003). Determining the exact timing of the calcrete development at Alapars-1 is, though, challenging because of the multi-episodic nature of calcrete formation (see Wright, 2007) and the absence of chronometric dates from the relevant deposits. However, based on the macroscale sedimentological evidence, it is hypothesised that calcrete formation at Alapars-1 would have occurred subsequent to aeolian deposition and is therefore likely to post-date the IRSL ages of Unit 2. Nevertheless, further geochemical and chronological study of the deposit is needed to fully elucidate the timing and nature of this formation.

Sedimentological evidence from Unit 2 indicates a complex depositional history comprising four main phases: (1) aeolian sedimentation, (2) formation of a gravel lag associated with fluvial deposition and later deflation of fine-grained material, (3) a return to aeolian sedimentation, and (4) carbonate precipitation associated with pedogenesis and the formation of Pedocomplex II. Aeolian material may have been transported from a number of local and regional sources, and while an absence of geochemical evidence from the aeolian deposits at Alapars-1 precludes an interpretation of likely sources, it is important to note that other aeolian deposits have been identified elsewhere in the Hrazdan Basin (Sherriff et al., 2019). The occurrence of a gravel lag indicates that, during this episode of aeolian deposition, fluvial systems may still have been active, albeit likely ephemeral in nature.

Units 1a and 1b represent the development of the uppermost strata that are overprinted by Pedocomplex II and which have been subjected to modern ploughing. Lithic Assemblage A was recovered from Unit 1 and contains exclusively MP artefacts most likely eroded or reworked from the top of Unit 2.

The chronological and environmental context of the Alapars-1 occupations

The current spatiotemporal distribution of MP sites in the Southern Caucasus and the Armenian highland may be a product of hominin settlement patterns, landscape abandonment, current research bias, or a mixture of these and other factors. Neither the connections between the distribution of sites and climatic oscillations, nor the interregional effects of environmental changes on population dynamics are clear. For example, the MIS 5e interglacial is regarded as a period during which *H. sapiens* dispersed out of Africa and into Eurasia (e.g., Groucutt et al., 2015). It has been suggested that major barriers to this dispersal, such as the Sahara Desert (northern Africa) and Negev Desert (Israel), became ecologically suitable and receptive to exchanges of faunal communities and human populations during that time (e.g., Vaks et al., 2007; Groucutt et al., 2015; Breeze et al., 2016; Frumkin and Comay, 2019). The most secure examples of *H. sapiens* ascribed to this phase are found in the Levant and include Qafzeh (Vandermeersch, 1981; Schwarcz et al., 1988; Valladas et al., 1988) and Skhul (McCown and Keith, 1939; Mercier et al., 1993; Grün et al., 2005). However, in recent years, the palaeoclimatic record in the Levant for the later stages of MIS 5 has been interpreted as a period of marked aridity (e.g., Neugebauer et al., 2016; Kiro et al., 2017; Palchan et al., 2017). In contrast to the palaeoclimatic proxies from Lake Lisan (the lacustrine forerunner of the present Dead Sea), the MIS 5 proxies from Lake Van suggest a shift to progressively warmer and wetter conditions within three periods of MIS 5: MIS 5e-d (124.1–111.5 ka); MIS 5c (107.8–87.2 ka), and MIS 5a (84.9–77.5 ka) (Pickarski et al., 2015a, 2015b; Kappenberg et al., 2019). The oscillations between these climatic periods likely triggered regional-to-local changes in the seasonal distribution of rainfall (see Rowe et al., 2012; Stockhecke et al., 2016). It has also been argued that climate, and specifically that of MIS 5, may not have been the determinant factor in the movement of hominin populations between Africa and Eurasia (Breeze et al., 2016; Timmermann and Friedrich, 2016; Greenbaum et al., 2018). Based on these data, it should be expected that during MIS 5 there would be widespread evidence for the occupation of the Armenian highlands and the Southern Caucasus, whereas during MIS 4 and 3, when climatic conditions became more arid, hominin occupation should be expected to be limited.

Lithic Assemblage A is currently the second assemblage that can be attributed to MIS 5 in the Armenian highlands and the Southern Caucasus. The other was recovered at the site of Hovk-1, Unit 8, where a small lithic assemblage was found in a mainly natural accumulation of faunal material located at high elevation (2000 m asl), (Pinhasi et al., 2008, 2011). Assemblage A appears to represent repeated brief episodes of artefact maintenance and use. This assemblage contains mainly small items whose preservation suggests they were subject to fast burial. Interestingly, no long-distance transport of raw material was detected, and the assemblage

derives completely from locally available raw material within the GVC, which falls within the expected daily foraging range of the site (Bailey and Davidson, 1983).

During MIS 4 (71–57 ka) and mostly during MIS 3 (57–29 ka), there is a relatively higher abundance of archaeological assemblages in the Armenian highlands and the Southern Caucasus in comparison to any previous period (e.g., Adler et al., 2008, 2012; Gasparyan et al., 2014; Moncel et al., 2015; Glauberman et al., 2016, 2020; Pleurdeau et al., 2016; Douka and Higham, 2017; Kandel et al., 2017). Assemblage B, dated to 63 ± 6 and 67 ± 7 ka, adds to this corpus of sites, but is older than most of the others. This assemblage has been affected by the winnowing of smaller artefacts, as well as a reoccurring cycle of burial, surface exposure, and reburial. Assemblage B also exhibits techno-typological characteristics that are different from the underlying Assemblage A. In Assemblage B, there are indications of on-site knapping as represented by nearly all stages of core reduction, including flake production and use. This variability cannot be explained solely by differences in the post-depositional processes between Assemblages A and B.

The sourced obsidian artefacts from Assemblage B do not derive only from the local GVC area. A small number of artefacts are made on obsidian from sources located beyond the approximately 25-km daily foraging range (Bailey and Davidson, 1983). Artefacts from obsidian sources closer to Alapars-1, namely the Hatis (ca. 10 km) and Tsaghkunyats sources (ca. 50 km), are represented by production classes of material. The most distant source (Pokr Arteni, ca. 75 km to the west as the crow flies and >100 km on foot) is represented by a retouched tool, conforming to the concept of individual provisioning (*sensu* Kuhn, 1995).

In contrast with Assemblage A, the diversity of obsidian sources in Assemblage B may indicate either more extensive foraging trips of potentially longer duration or obsidian procurement, artefact manufacture, and use in the course of residential mobility by individuals equipped with mobile tool kits (*sensu* Binford, 1979; Kuhn, 1995). Most obsidian exploitation appears to have been associated with mobility and foraging forays within the daily exploration territory, while the longest obsidian transport distance was likely related to the social landscapes that extend beyond the immediate foraging scales (Tindale, 1974; Gamble, 1999). At the penecontemporaneous site of Lusakert-1 cave in the Hrazdan River valley and at the open-air site of Barozh 12 near the Arteni obsidian sources, similar raw material economies were observed (Frahm et al., 2016; Glauberman et al., 2016).

The results from Alapars-1 suggest that during the ameliorated conditions of MIS 5, hominins ephemerally occupied the locality. A similar signature of ephemeral occupation was observed at the penecontemporaneous site of Hovk-1 (Pinhasi et al., 2011). The emerging pattern could, therefore, be interpreted as signifying that either MIS 5 was a period characterised by low population densities, or alternatively that the lack of sites attributed to this time period is a result of taphonomic bias and/or limited research in the region. Similar interpretive scenarios have been discussed in the Western European

record for the last interglacial, MIS 5e (e.g., Defleur and Desclaux, 2019; Defleur et al., 2020; vs. Slimak and Nicholson, 2020 debating those different interpretive scenarios).

During the glacial and interstadial periods (MIS 4–3) between ca. 71 and 29 ka, climates were generally drier and cooler, yet had intervals of warm and wetter conditions (Stockhecke et al., 2016). During this period, occupation intensity, as documented in the number of sites and artefact densities, was apparently more substantial in the region.

CONCLUSIONS

This paper reports the findings from combined lithostratigraphic, chronometric, and archaeological analyses at the MP site of Alapars-1 in central Armenia. The site is situated in sedimentary deposits that cover an extrusive obsidian-rhyolitic dome within the GVC, is located at a high elevation of 1774 m asl, and contains lithic artefact assemblages indicative of the changing role of this locale within regional MP settlement systems. The Alapars-1 sequence provides evidence for three periods of MP occupation and changes in depositional environment during the MIS 5–3 interval.

The MIS 5 archaeological assemblages were recovered from a compound palaeosol that developed in an alluvial setting and suggest ephemeral occupations, with a focus on tool use and maintenance. Obsidian sourcing indicates utilisation of only locally occurring GVC obsidian. MIS 5 is regarded in eastern Anatolia as a period of warm, humid climates (Litt et al., 2014; Pickarski et al., 2015a), but despite the resource-rich landscapes that likely resulted, Alapars-1 is only the second site in the region dating to this time interval. Other documented exposures in Armenia with well-developed compound palaeosols and associated biomarker evidence also indicate a relatively warm and stable climate during MIS 5 (e.g., Wolf et al., 2016; Trigui et al., 2019; Richter, 2020). In contrast, during MIS 4–3, when climatic conditions are likely to have been more arid and less stable in the region (Pickarski et al., 2015b; Stockhecke et al., 2016; Wolf et al., 2016; Trigui et al., 2019; Richter, 2020), hominin occupations at Alapars-1 were more intensive than those documented during MIS 5. Lithic artefact assemblages of the latter document nearly all stages of core reduction, showing an emphasis on blank production, use, and maintenance. Indeed, despite a complex formation history during MIS 4–3, longer duration or more frequent occupations are documented, suggesting an evolving use of the locality over time. The MIS 4–3 artefact assemblages are produced on both local and distant obsidian sources, suggesting an obsidian exploitation territory that extended over a wide geographic area (the most distant raw material is located more than 100 km away on foot). It is worth noting that obsidian sourcing at regional MP sites indicates the long-distance exploitation of the same obsidian sources, with overlapping artefact transports among source areas and archaeological sites (Frahm et al., 2014, 2016; Glauberman et al., 2016, 2020). This pattern suggests that extensive social networks were well established in

this region during MIS 4–3. Mobility over large territories represents an adaptive coping mechanism that minimizes the risk of seasonal and decadal resource fluctuation and depletion (Kuhn et al., 2016).

The record from Alapars-1 adds to the growing corpus of widespread evidence of MP occupation of the Armenian highland and Southern Caucasus during MIS 4–3. The current MP record indicates that throughout the fluctuating environmental conditions of MIS 5–3 hunter-gatherers were well adapted to a diverse array of biomes that were segregated by sharp topographic gradients. MP sites of variable size and density with artefact and faunal assemblages have been documented in palaeo-lake margins in basins, fluvial/floodplain settings in a variety of topographic positions, and ecotones between mountain ranges and basins (Adler et al., 2006; Ghukasyan et al., 2011; Pinhasi et al., 2011; Gasparian et al., 2014; Moncel et al., 2015; Egeland et al., 2016; Frahm et al., 2016; Sherriff et al., 2019; Glauber et al., 2020). Alapars-1 documents repeated but variable high-elevation occupations, thus broadening our understanding of the range of niches MP hominins were capable of exploiting in the rugged and ecologically diverse terrain of the Armenian highland.

ACKNOWLEDGMENTS

We thank Pavel Avetisyan, Director of the Institute for Archaeology and Ethnography, National Academy of Sciences, Republic of Armenia, for his continued support of our research. We also thank Suren Kesejyan, Hovik Partevyan, Artur Petrosyan, Avetis Grigoryan, Samvel Nahapetyan, and the University of Connecticut students who worked at the site. Figures 6–9 were drawn and photographed by Garik Prevyan and Dmitri Arakelyan. We also wish to thank Karen Bayramyan, Head of the Protection of Monuments of History and Culture Agency for the Kotayk and Gegharkunik Provinces, the Ministry of Culture, Republic of Armenia, for his assistance during the fieldwork activities. AMB wishes to thank the Fulbright Postdoctoral Fellowship Program. The excavations and analyses were funded by the Leverhulme Trust (Grant RPG-2016-102), the University of Winchester, and the University of Connecticut's Norian Armenian Programs Committee and the Gfoeller Renaissance Foundation, USA. We are grateful to the editors and anonymous reviewers who provided invaluable suggestions that greatly improved the quality of this paper.

SUPPLEMENTARY MATERIAL

The supplementary material for this article can be found at <https://doi.org/10.1017/qua.2020.61>

REFERENCES

- Adler, D.S., Bar-Oz, G., Belfer-Cohen, A., Bar-Yosef, O., 2006. Ahead of the game: Middle and Upper Palaeolithic hunting behaviors in the southern Caucasus. *Current Anthropology* 47, 89–118. <https://doi.org/10.1086/432455>.
- Adler, D.S., Bar-Yosef, O., Belfer-Cohen, A., Tushabramishvili, N., Boaretto, E., Mercier, N., Valladas, H., Rink, W.J., 2008. Dating the demise: Neandertal extinction and the establishment of modern humans in the southern Caucasus. *Journal of Human Evolution* 55, 817–833. <https://doi.org/10.1016/j.jhevol.2008.08.010>.
- Adler, D.S., Wilkinson, K.N., Blockley, S., Mark, D.F., Pinhasi, R., Schmidt-Magee, B.A., Nahapetyan, S., et al., 2014. Early Levallois technology and the Lower to Middle Paleolithic transition in the Southern Caucasus. *Science* 345, 1609–1613. <https://doi.org/10.1126/science.1256484>.
- Adler, D.S., Yeritsyan, B., Wilkinson, K., Pinhasi, R., Bar-Oz, G., Nahapetyan, S., Bailey, R., et al., 2012. The Hrazdan Gorge Palaeolithic Project, 2008–2009. In: Avetisyan, P., Bobokhyan, A. (Eds.), *Archaeology of Armenia in Regional Context. Proceedings of the International Conference Dedicated to the 50th Anniversary of the Institute of Archaeology and Ethnography Held on September 15–17, 2009 in Yerevan, Armenia*. NAS RA Gitutyn Publishing House, Yerevan, pp. 21–37.
- Aitken, M.J., 1998. *An Introduction to Optical Dating: The Dating of Quaternary Sediments by the Use of Photon-stimulated Luminescence*. Oxford University Press, Oxford.
- Alonso-Zarza, A.M., Silva, P.G., 2002. Quaternary laminar calcretes with bee nests: evidences of small-scale climatic fluctuations, Eastern Canary Islands, Spain. *Palaeogeography, Palaeoclimatology, Palaeoecology* 178, 119–135. [https://doi.org/10.1016/S0031-0182\(01\)00405-9](https://doi.org/10.1016/S0031-0182(01)00405-9).
- Alonso-Zarza, A.M., Wright, V.P., 2010. Calcretes. *Developments in Sedimentology* 61, 225–267.
- Anovitz, L.M., Elam, J.M., Riciputi, L.R., Cole, D.R., Fayek, M., 2006. Obsidian hydration: a new paleothermometer. *Geology* 34, 517–520. <https://doi.org/10.1130/G22326.1>.
- Arenas-Abad, C., Vázquez-Urbez, M., Pardo-Tirapu, G., Sancho-Marcén, C., 2010. Fluvial and associated carbonate deposits. *Developments in Sedimentology* 61, 133–175. [https://doi.org/10.1016/S0070-4571\(09\)06103-2](https://doi.org/10.1016/S0070-4571(09)06103-2).
- Arutyunyan, E.V., Lebedev, V.A., Chernyshev, I.V., Sagatelyan, A.K., 2007. Geochronology of Neogene-Quaternary volcanism of the Geghama Highland (Lesser Caucasus, Armenia). *Doklady Earth Sciences* 416, 1042–1046. <https://doi.org/10.1134/S1028334X07070136>.
- Badalian, R., Bigazzi, G., Cauvin, M.C., Chataigner, C., Jrbashyan, R., Karapetyan, S.G., Oddone, M., Poidevin, J.L., 2001. An international research project on Armenian archaeological sites: fission-track dating of obsidians. *Radiation Measurements* 34, 373–378. [https://doi.org/10.1016/S1350-4487\(01\)00189-5](https://doi.org/10.1016/S1350-4487(01)00189-5).
- Bailey, G.N., Davidson, I., 1983. Site exploitation of territories and topography: two case studies from Palaeolithic Spain. *Journal of Archaeological Science* 10, 87–116. [https://doi.org/10.1016/0305-4403\(83\)90044-4](https://doi.org/10.1016/0305-4403(83)90044-4).
- Bar-Oz, G., Weissbrod, L., Gasparian, B., Nahapetyan, S., Wilkinson, K., Pinhasi, R., 2012. Taphonomy and zooarchaeology of a high-altitude Upper Pleistocene faunal sequence from Hovk-1 Cave, Armenia. *Journal of Archaeological Science* 39, 2452–2463. <https://doi.org/10.1016/j.jas.2012.02.014>.
- Bar-Yosef, O., 1981. The Epi-Palaeolithic complexes in the Southern Levant. In: Cauvin, P., Sanlaville, J. (Eds), *Préhistoire Du Levant*. CNRS, Paris, pp. 389–408.
- Binford, L.R., 1979. Organization and formation processes: looking at curated technologies. *Journal of Anthropological Research* 35, 255–273.
- Blockley, S.P.E., Pyne-O'Donnell, S.D.F., Lowe, J.J., Matthews, I.P., Stone, A., Pollard, A.M., Turney, C.S.M., Molyneux, E.G., 2005. A new and less destructive laboratory procedure for the physical separation of distal glass tephra shards from sediments.

- Quaternary Science Reviews* 24, 1952–1960. <https://doi.org/10.1016/j.quascirev.2004.12.008>.
- Boëda, E., 1995. Levallois: a volumetric construction, methods, a technique. In: Dibble, H.L., Bar-Yosef, O. (Eds.), *The Definition and Interpretation of Levallois Technology*. Monographs in World Archaeology, Ann-Arbor, pp. 41–68.
- Bordes, F., 1961. *Typologie du Paléolithique Ancien et Moyen*. CNRS, Paris.
- Bøtter-Jensen, L., McKeever, S.W., Wintle, A.G., 2003. *Optically Stimulated Luminescence Dosimetry*. Elsevier.
- Breeze, P.S., Groucutt, H.S., Drake, N.A., White, T.S., Jennings, R.P., Petraglia, M.D., 2016. Palaeohydrological corridors for hominin dispersals in the Middle East ~250–70,000 years ago. *Quaternary Science Reviews* 144, 155–185. <https://doi.org/10.1016/j.quascirev.2016.05.012>.
- Burroni, D., Donahue, R.E., Pollard, A.M., Mussi, M., 2002. The surface alteration features of flint artefacts as a record of environmental processes. *Journal of Archaeological Science* 29, 1277–1287. <https://doi.org/10.1006/jasc.2001.0771>.
- Candy, I., Black, S., Sellwood, B.W., Rowan, J.S., 2003. Calcrete profile development in Quaternary alluvial sequences, southeast Spain: implications for using calcretes as a basis for landform chronologies. *Earth Surface Processes and Landforms* 28, 169–185. <https://doi.org/10.1002/esp.445>.
- Davies, S. M., Cryptotephros: the revolution in correlation and precision dating. 2015. *Journal of Quaternary Science* 30, 114–130. doi:10.1002/jqs.2766
- Dearing, J., 1999. *Environmental Magnetic Susceptibility: Using the Bartington MS2 System*. Chi Publishing, Kenilworth.
- Defleur, A.R., Desclaux, E., 2019. Impact of the last interglacial climate change on ecosystems and Neanderthals behavior at Baume Moula-Guercy, Ardèche, France. *Journal of Archaeological Science* 104, 114–124. <https://doi.org/10.1016/j.jas.2019.01.002>.
- Defleur, A.R., Desclaux, E., Jabbour, R.S., Richards, G.D., 2020. The Eemian: global warming, ecosystem upheaval, demographic collapse and cannibalism at Moula-Guercy. A reply to Slimak and Nicholson (2020). *Journal of Archaeological Science* 117, 105113. <https://doi.org/10.1016/j.jas.2020.105113>.
- Delagnes, A., 2000. Blade production during the Middle Paleolithic in northwestern Europe. *Acta Anthropologica Sinica* 19, 169–176.
- Djamali, M., de Beaulieu, J.-L., Shah-hosseini, M., Andrieu-Ponel, V., Ponel, P., Amini, A., Akhiani, H., et al., 2008. A Late Pleistocene long pollen record from the Urmia Lake, North Western Iran. *Quaternary Research* 69, 413–420. <https://doi.org/10.1016/j.yqres.2008.03.004>.
- Douka, K., Higham, T., 2017. The chronological factor in understanding the Middle and Upper Palaeolithic of Eurasia. *Current Anthropology* 58, S480–S490. <https://doi.org/10.1086/694173>.
- Egeland, C. P., Gasparian, B., Fadem, C.M., Nahapetyan, S., Arakelyan, D., Nicholson, C.M., 2016. Bagratashen 1, a stratified open-air Middle Paleolithic site in the Debed river valley of north-eastern Armenia: A preliminary report. *Archaeological Research in Asia*, 8, 1–20. doi:10.1016/j.ara.2016.10.001
- Fedoroff, N., Courty, M.A., Lacroix, E., Oleschko, K., 1994. Calcitic accretion on indurated volcanic materials (example of tepetates, Altiplano, Mexico). *Transactions of the 15th World Congress of Soil Science, Acapulco, Mexico*, 6a, 460–473.
- Fink, J.H., 1983. Structure and emplacement of a rhyolitic obsidian flow: Little Glass Mountain, Medicine Lake Highland, northern California. *Geological Society of American Bulletin* 94, 262–280.
- Folk, R.L., Ward, W.C., 1957. Brazos River bar [Texas]; a study in the significance of grain size parameters. *Journal of Sedimentary Research* 27, 3–26. <https://doi.org/10.1306/74D70646-2B21-11D7-8648000102C1865D>.
- Frahm, E., 2014. Characterizing obsidian sources with portable XRF: accuracy, reproducibility, and field relationships in a case study from Armenia. *Journal of Archaeological Science* 49, 105–125. <https://doi.org/10.1016/j.jas.2014.05.003>.
- Frahm, E., 2016. Can I get chips with that? Sourcing small obsidian artifacts down to microdebitage scales with portable XRF. *Journal of Archaeological Science: Reports* 9, 448–467. <https://doi.org/10.1016/j.jasrep.2016.08.032>.
- Frahm, E., Feinberg, J.M., 2015. Reassessing obsidian field relationships at Glass Buttes, Oregon. *Journal of Archaeological Science: Reports* 2, 654–665. <https://doi.org/10.1016/j.jasrep.2014.11.007>.
- Frahm, E., Feinberg, J.M., Schmidt-Magee, B.A., Wilkinson, K., Gasparyan, B., Yeritsyan, B., Adler, D.S., 2016. Middle Palaeolithic toolstone procurement behaviors at Lusakert Cave 1, Hrazdan Valley, Armenia. *Journal of Human Evolution* 91, 73–92. <https://doi.org/10.1016/j.jhevol.2015.10.008>.
- Frahm, E., Feinberg, J.M., Schmidt-Magee, B.A., Wilkinson, K., Gasparyan, B., Yeritsyan, B., Karapetian, S., Meliksetian, K., Muth, M.J., Adler, D.S., 2014. Sourcing geochemically identical obsidian: multiscale magnetic variations in the Gutansar Volcanic Complex and implications for Palaeolithic research in Armenia. *Journal of Archaeological Science* 47, 164–178. <https://doi.org/10.1016/j.jas.2014.04.015>.
- Frumkin, A., Comay, O., 2019. The last glacial cycle of the southern Levant: paleoenvironment and chronology of modern humans. *Journal of Human Evolution*. <https://doi.org/10.1016/j.jhevol.2019.04.007>.
- Gale, S.J., Hoare, P.G., 1991. *Quaternary Sediments*. Belhaven Press, London.
- Gamble, C., 1999. *The Palaeolithic Societies of Europe*. Cambridge University Press, Cambridge.
- Gasparyan, B., Egeland, C.P., Adler, D.S., Pinhasi, R., Glauberman, P., Haydosyan, H., 2014. The Middle Paleolithic occupation of Armenia: summarizing old and new data. In: Gasparyan, B., Arimura, M. (Eds.), *Stone Age of Armenia: A Guide-Book to the Stone Age Archaeology in the Republic of Armenia*. Kanazawa University Press, Kanazawa, pp. 65–105.
- Geneste, J.-M., 1985. *Analyse d'industries Moustériennes du Périgord: Une Approche Technologique du Comportement des Groupes Humains Paléolithique Moyen*. University of Bordeaux, Bordeaux.
- Genise, J.F., Alonso-Zarza, A.M., Verde, M., Meléndez, A., 2013. Insect trace fossils in aeolian deposits and calcretes from the Canary Islands: Their ichnotaxonomy, producers, and palaeoenvironmental significance. *Palaeogeography Palaeoclimatology Palaeoecology*, 377, 110–124. doi:10.1016/j.palaeo.2013.03.005
- Ghukasyan, R., Colonge, D., Nahapetyan, S., Ollivier, V., Gasparyan, B., Monchot, H., Chataigner, C., 2011. Kalavan-2 (north of lake Sevan, Armenia): A new late Middle Paleolithic site in the Lesser Caucasus. *Archaeological, Ethnological and Anthropological Eurasia* 38, 39–51. <https://doi.org/10.1016/j.aear.2011.02.003>.
- Glauberman, P., Gasparyan, B., Sherriff, J., Wilkinson, K., Li, B., Knul, M., Brittingham, A., et al., 2020. Barozh 12: formation processes of a late Middle Paleolithic open-air site in western Armenia. *Quaternary Science Reviews* 236. <https://doi.org/10.1016/j.quascirev.2020.106276>.
- Glauberman, P., Gasparyan, B., Wilkinson, K., Frahm, E., Raczynski-Henk, Y., Haydosyan, H., Arakelyan, D., Karapetyan,

- S., Nahapetyan, S., Adler, D., 2016. Introducing Barozh 12: A Middle Palaeolithic open-air site on the edge of the Ararat Depression, Armenia. *ARAMAZD-Armenian Journal of Near Eastern Studies* IX (2), 7–20.
- Glauberger, P., Thorson, R.M., 2012. Flint patina as an aspect of flaked stone taphonomy. *Journal of Taphonomy* 10, 21–43.
- Goudie, A.S., 1983. Calcrete. In: Goudie, A.S., Pye, K. (Eds.), *Chemical Sediments and Geomorphology: Precipitates and Residua in the Near Surface Environment*. Academic Press, London, p. 439.
- Greenbaum, G., Kolodny, O., Hovers, E., Feldman, M.W., Friesem, D.E., 2018. Was inter-population connectivity of Neanderthals and modern humans the driver of the Upper Paleolithic transition rather than its product? *Quaternary Science Reviews* 217, 316–329. <https://doi.org/10.1016/j.quascirev.2018.12.011>.
- Groucutt, H.S., Petraglia, M.D., Bailey, G., Scerri, E.M., Parton, A., Clark-Balzan, L., Jennings, R. P., et al., 2015. Rethinking the dispersal of Homo Sapiens out of Africa. *Evolutionary Anthropology: Issues, News, and Reviews* 24, 149–164. <https://doi.org/10.1002/evan.21455>.
- Grün, R., Stringer, C., McDermott, F., Nathan, R., Porat, N., Robertson, S., Taylor, L., Mortimer, G., Eggins, S., McCulloch, M., 2005. U-series and ESR analyses of bones and teeth relating to the human burials from Skhul. *Journal of Human Evolution* 49, 316–334. <https://doi.org/10.1016/j.jhevol.2005.04.006>.
- Hovers, E., 2009. *The Lithic Assemblages of Qafzeh Cave*. Oxford University Press, Oxford.
- Huerta, P., Rodríguez-Berriguete, Á., Martín-García, R., Martín-Pérez, A., Fernández, Á.L.I., Alonso-Zarza, A.M., 2015. The role of climate and aeolian dust input in calcrete formation in volcanic islands (Lanzarote and Fuerteventura, Spain). *Palaeogeography, Palaeoclimatology, Palaeoecology* 417, 66–79. <https://doi.org/10.1016/j.palaeo.2014.10.008>.
- Kandel, A.W., Gasparian, B., Allué, A., Bigga, G., Bruch, A.A., Cullen, V.L., Frahm, E., et al., 2017. The earliest evidence for Upper Paleolithic occupation in the Armenian highlands at Aghitu-3 Cave. *Journal of Human Evolution* 110, 37–68. <https://doi.org/10.1016/j.jhevol.2017.05.010>.
- Kappenberg, A., Lehdorff, E., Pickarski, N., Litt, T., Amelung, W., 2019. Solar controls of fire events during the past 600,000 years. *Quaternary Science Reviews* 208, 97–104. <https://doi.org/10.1016/j.quascirev.2019.02.008>.
- Karapetian, S.G., Jrbashian, R.T., Mnatsakanian, A.Kh., 2001. Late collision rhyolitic volcanism in the north-eastern part of the Armenian highland. *Journal of Volcanology and Geothermal Research* 112, 189–220. [https://doi.org/10.1016/S0377-0273\(01\)00241-4](https://doi.org/10.1016/S0377-0273(01)00241-4).
- Kiro, Y., Goldstein, S.L., Garcia-Veigas, J., Levy, E., Kushnir, Y., Stein, M., Lazar, B., 2017. Relationships between lake-level changes and water and salt budgets in the Dead Sea during extreme aridities in the Eastern Mediterranean. *Earth and Planetary Science Letters* 464, 211–226. <https://doi.org/10.1016/j.epsl.2017.01.043>.
- Knox, G.J., 1977. Caliche profile formation, Saldanha Bay (South Africa). *Sedimentology* 24, 657–674. <https://doi.org/10.1002/9781444304497.ch4>.
- Kuhn, S.L., 1995. *Mousterian Lithic Technology: An Ecological Perspective*. Princeton University Press, Princeton.
- Kuhn, S.L., Raichlen, D.A., Clark, A.E., 2016. What Moves Us? How Mobility and Movement Are at the Center of Human Evolution. *Evolutionary Anthropology: Issues, News, and Reviews* 25, 86–97. <https://doi.org/10.1002/evan.21480>.
- Lane, C.S., Cullen, V.L., White, D., Bramham-Law, C.W.F., Smith, V.C., 2014. Cryptotephra as a dating and correlation tool in archaeology. *Journal of Archaeological Science* 42, 42–50. <https://doi.org/10.1016/j.jas.2013.10.033>.
- Lebedev, V.A., Chernyshev, I.V., Sagatelyan, A.K., Goltsman, Yu.V., Oleinikova, T.I., 2018. Miocene–Pliocene volcanism of central Armenia: geochronology and the role of AFC processes in magma petrogenesis. *Journal of Volcanology and Seismology* 12, 310–331. <https://doi.org/10.1134/S0742046318050056>.
- Lebedev, V.A., Chernyshev, I.V., Shatagin, K.N., Bubnov, S.N., Yakushev, A.I., 2013. The Quaternary volcanic rocks of the Geghama Highland, Lesser Caucasus, Armenia: Geochronology, isotopic Sr-Nd characteristics, and origin. *Journal of Volcanology and Seismology* 7, 204–229. <https://doi.org/10.1134/S0742046313030044>.
- Lebedev, V.A., Chernyshev, I.V., Yakushev, A.I., 2011. Initial time and duration of Quaternary magmatism in the Aragats neovolcanic area (Lesser Caucasus, Armenia). *Doklady Earth Sciences* 437, 532–536. <https://doi.org/10.1134/S1028334X11040209>.
- Litt, T., Pickarski, N., Heumann, G., Stockhecke, M., Tzedakis, P.C., 2014. A 600,000 year long continental pollen record from Lake Van, Eastern Anatolia (Turkey). *Quaternary Science Reviews* 104, 30–41. <https://doi.org/10.1016/j.quascirev.2014.03.017>.
- Lowe, D.J., Hunt, J.B., 2001. A summary of terminology used in tephra-related studies. *Les Dossiers de l'Archéo-Logis* 1, 17–22.
- Mather, A.E., Stokes, M., Whitfield, E., 2017. River terraces and alluvial fans: the case for an integrated Quaternary fluvial archive. *Quaternary Science Reviews* 166, 74–90. <https://doi.org/10.1016/j.quascirev.2016.09.022>.
- McCown, T.D., Keith, A., 1939. *The Stone Age of Mt. Carmel II, The Fossil Human Remains from the Levalloiso-Mousterian*. Clarendon Press, Oxford.
- McPhie, J., Doyle, M., Allen, R., 1993. *Volcanic Textures. A Guide to the Interpretation of Textures in Volcanic Rocks*. University of Tasmania, Tasmania.
- Meignen, L., 1998. A preliminary report on Hayonim Cave lithic assemblages in the context of the Near Eastern Middle Palaeolithic. In: Bar-Yosef, O., Akazawa, T., Aoki, T. (Eds.), *Humans in Western Asia*. Plenum Press, New York, pp. 165–180.
- Meléndez, A., Alonso-Zarza, A.M., Sancho, C., 2011. Multi-storey calcrete profiles developed during the initial stages of the configuration of the Ebro Basin's exorheic fluvial network. *Geomorphology* 134, 232–248. <https://doi.org/10.1016/j.geomorph.2011.06.032>.
- Mercier, N., Valladas, H., Bar-Yosef, O., Vandermeersch, B., Stringer, C., Joron, J.L., 1993. Thermoluminescence date for the Mousterian burial site of Es-Skhul, Mt. Carmel. *Journal of Archaeological Science* 20, 169–74.
- Mercier, N., Valladas, H., Meignen, L., Joron, J.-L., Tushabramishvili, N., 2010. Dating the early Middle Palaeolithic laminar industry from Djruchula Cave, Republic of Georgia. *Paléorient* 36, 163–173. <https://doi.org/10.1006/jasc.1993.1012>.
- Mitchell, J., Westaway, R., 1999. Chronology of Neogene and Quaternary uplift and magmatism in the Caucasus: constraints from K–Ar dating of volcanism in Armenia. *Tectonophysics* 304, 157–186. [https://doi.org/10.1016/S0040-1951\(99\)00027-X](https://doi.org/10.1016/S0040-1951(99)00027-X).
- Moncel, M.-H., Pleurdeau, D., Pinhasi, R., Yeshurun, R., Agapishvili, T., Chevalier, T., Lebourdonnec, F.-X., et al., 2015. The Middle Palaeolithic record of Georgia: a synthesis of the technological, economic and paleoanthropological aspects. *Anthropologie* LIII, 93–125.

- Neugebauer, I., Schwab, M.J., Waldmann, N.D., Tjallingii, R., Frank, U., Hadzhiivanova, E., Naumann, R., et al., 2016. Hydroclimatic Variability in the Levant during the early last glacial (~117–75 Ka) derived from micro-facies analyses of deep Dead Sea sediments. *Climate of the Past* 12, 75–90. <https://doi.org/10.5194/cp-12-75-2016>.
- Palchan, D., Neugebauer, I., Amitai, Y., Waldmann, N.D., Schwab, M.J., Dulski, P., Brauer, A., Stein, M., Erel, Y., Enzel, Y., 2017. North Atlantic controlled depositional cycles in MIS 5e layered sediments from the deep Dead Sea basin. *Quaternary Research* 87, 168–179. <https://doi.org/10.1017/qua.2016.10>.
- Pentecost, A., 2005. *Travertine*. Springer, New York.
- Petraglia, M.D., Potts, R., 1994. Water flow and the formation of early Pleistocene artifact sites in Olduvai Gorge. *Journal of Anthropological Archaeology* 13, 228–254. <https://doi.org/10.1006/jaar.1994.1014>.
- Pickarski, N., Kwiecien, O., Langgut, D., Djamali, M., Litt, T., 2015a. Vegetation and environmental changes during the last interglacial in eastern Anatolia (Turkey): a new high-resolution pollen record from Lake Van. *Palaeogeography, Palaeoclimatology, Palaeoecology* 435, 145–158. <https://doi.org/10.1016/j.palaeo.2015.06.015>.
- Pickarski, N., Kwiecien, O., Langgut, D., Litt, T., 2015b. Abrupt climate and vegetation variability of eastern Anatolia during the last glacial. *Climate of the Past* 11, 1491–1505. <https://doi.org/10.5194/cp-11-1491-2015>.
- Pickarski, N., Litt, T., 2017. A new high-resolution pollen sequence at Lake Van, Turkey: insights into penultimate interglacial-glacial climate change on vegetation history. *Climate of the Past* 13, 689–710. <https://doi.org/10.5194/cp-13-689-2017>.
- Pinhasi, R., Gasparian, B., Nahapetyan, S., Bar-Oz, G., Weissbrod, L., Bruch, A.A., Hovsepian, R., Wilkinson, K., 2011. Middle Palaeolithic human occupation of the high altitude region of Hovk-1, Armenia. *Quaternary Science Reviews* 30, 3846–3857. <https://doi.org/10.1016/j.quascirev.2011.09.020>.
- Pinhasi, R., Gasparian, B., Wilkinson, K., Bailey, R., Bar-Oz, G., Bruch, A.A., Chataigner, C., et al., 2008. Hovk 1 and the Middle and Upper Paleolithic of Armenia: A preliminary framework. *Journal of Human Evolution* 55, 803–816. <https://doi.org/10.1016/j.jhevol.2008.04.005>.
- Pleurdeau, D., Moncel, M.H., Pinhasi, R., Yeshurun, R., Higham, T., Agapishvili, T., Bokeria, M., et al., 2016. Bondi Cave and the Middle-Upper Palaeolithic transition in western Georgia (South Caucasus). *Quaternary Science Reviews* 146, 77–98. <https://doi.org/10.1016/j.quascirev.2016.06.003>.
- Randlett, M.-E., Bechtel, A., van der Meer, M.T.J., Peterse, F., Litt, T., Pickarski, N., Kwiecien, O., Stockhecke, M., Wehrli, B., Schubert, C.J., 2017. Biomarkers in Lake Van sediments reveal dry conditions in eastern Anatolia during 110,000–10,000 years B.P. *Geochemistry, Geophysics, Geosystems* 18, 571–583. <https://doi.org/10.1002/2016GC006621>.
- Richter, C., Wolf, D., Walther, F., Meng, S., Sahakyan, L., Hovakimyan, H., Wolpert, T., Fuchs, M., Faust, D., 2020. New Insights into Southern Caucasian Glacial–Interglacial Climate Conditions Inferred from Quaternary Gastropod Fauna. *Journal of Quaternary Science*, <https://doi.org/10.1002/jqs.3204>.
- Rowe, P.J., Mason, J.E., Andrews, J.E., Marca, A.D., Thomas, L., Van Calsteren, P., Jex, C.N., Vonhof, H.B., Al-Omari, S., 2012. Speleothem isotopic evidence of winter rainfall variability in northeast Turkey between 77 and 6 Ka. *Quaternary Science Reviews* 45, 60–72. <https://doi.org/10.1016/j.quascirev.2012.04.013>.
- Schick, D.K., 1986. *Stone Age Sites in the Making: Experiments in the Formation and Transformation of Archaeological Occurrences*. BAR 319, International Series Oxford.
- Schroëder, B., 1969. *The Lithic Industries from Jerf Ajla and their Bearing on the Problem of a Middle to Upper Paleolithic Transition*. New York: Columbia University. (Unpublished PhD thesis).
- Schwarz, H.P., Grun, R., Vandermeersch, B., Bar-Yosef, O., Valladas, H., Tchernov, E., 1988. ESR dates for the hominid burial site of Qafzeh in Israel. *Journal of Human Evolution* 17, 733–737. [https://doi.org/10.1016/0047-2484\(88\)90063-2](https://doi.org/10.1016/0047-2484(88)90063-2).
- Shackley, M.L., 1974. Stream abrasion of chert implements. *Nature* 248, 501–502. <https://doi.org/10.1038/248501a0>.
- Sherriff, J.E., Wilkinson, K.N., Adler, D.S., Arakelyan, D., Beverly, E.J., Blockley, S.P.E., Gasparyan, B., et al., 2019. Pleistocene volcanism and the geomorphological record of the Hrazdan valley, central Armenia: linking landscape dynamics and the Palaeolithic record. *Quaternary Science Review* 226. <https://doi.org/10.1016/j.quascirev.2019.105994>.
- Slimak, L., Nicholson, C., 2020. Cannibals in the forest: a comment on Defleur and Desclaux (2019). *Journal of Archaeological Science* 117, 105034. <https://doi.org/10.1016/j.jas.2019.105034>.
- Solecki, R.L., Solecki, R., 1970. A new secondary site, flaking technique at the Nahr Ibrahim Cave, Lebanon. *Bulletin du Musée de Beyrouth* 23, 137–142.
- Stevens, L.R., Djamali, M., Andrieu-Ponel, V., Louis de Beaulieu, J., 2012. Hydroclimatic variations over the last two glacial/interglacial cycles at Lake Urmia, Iran. *Journal of Paleolimnology* 47, 645–660. <https://doi.org/10.1007/s10933-012-9588-3>.
- Stewart, A.L., McPhie, J., 2003. Internal structure and emplacement of an Upper Pliocene dacite cryptodome, Milos Island, Greece. *Journal of Volcanology and Geothermal Research* 124, 129–148. [https://doi.org/10.1016/S0377-0273\(03\)00074-X](https://doi.org/10.1016/S0377-0273(03)00074-X).
- Stockhecke, M., Sturm, M., Brunner, I., Schmincke, H.U., Sumita, M., Kipfer, R., Cukur, D., Kwiecien, O., Anselmetti, F.S., 2014. Sedimentary evolution and environmental history of Lake Van (Turkey) over the past 600 000 years. *Sedimentology* 61, 1830–1861. <https://doi.org/10.1111/sed.12118>.
- Stockhecke, M., Timmermann, A., Kipfer, R., Haug, G.H., Kwiecien, O., Friedrich, T., Menviel, L., Litt, T., Pickarski, N., Anselmetti, F.S., 2016. Millennial to orbital-scale variations of drought intensity in the eastern Mediterranean. *Quaternary Science Reviews* 133, 77–95.
- Timmermann, A., Friedrich, T., 2016. Late Pleistocene climate drivers of early human migration. *Nature* 538, 92–95. <https://doi.org/10.1016/j.quascirev.2015.12.016>.
- Tindale, N.B., 1974. *Aboriginal Tribes of Australia: Their Terrain, Environmental Controls, Distribution, Limits, and Proper Names*. University of California Press, Berkeley.
- Trigui, Y., Wolf, D., Sahakyan, L., Hovakimyan, H., Sahakyan, K., Zech, R., Fuchs, M., Wolpert, T., Zech, M., Faust, D., 2019. First calibration and application of leaf wax *n*-alkane biomarkers in loess-paleosol sequences and modern plants and soils in Armenia. *Geosciences* 9, 263. doi:10.3390/geosciences9060263.
- Vaks, A., Bar-Matthews, M., Ayalon, A., Matthews, A., Halicz, L., Frumkin, A., 2007. Desert speleothems reveal climatic window for African exodus of early modern humans. *Geology* 35, 831–834. <https://doi.org/10.1130/G23794A.1>.
- Valladas, H., Reyss, J.-L., Joron, J.-L., Valladas, G., Bar-Yosef, O., Vandermeersch, B., 1988. Thermoluminescence dating of Mousterian ‘proto-Cro-Magnon’ remains from Israel and the origin of modern man. *Nature* 334, 614–616. <https://doi.org/10.1038/331614a0>.
- Vandermeersch, B., 1981. *Les Hommes Fossiles de Qafzeh, Israël*. CNRS, Paris.

- Villa, P., Courtin, J., 1983. The interpretation of stratified sites: a view from underground. *Journal of Archaeological Science* 10, 267–281. [https://doi.org/10.1016/0305-4403\(83\)90011-0](https://doi.org/10.1016/0305-4403(83)90011-0).
- Volodicheva, N., 2002. The Caucasus. In: Shahgedanova, M. (Ed.), *The Physical Geography of Northern Eurasia*. Oxford University Press, Oxford, pp. 350–376.
- Walkley, A., Black, I.A., 1934. An examination of the Degtjareff method for determining soil organic matter, and a proposed modification of the chromic acid titration method. *Soil Science* 37, 29–38.
- Walling, D.E., Fang, D., Nicholas, A.P., Sweet, R.J., 2004. The grain size characteristics of overbank deposits on the floodplains of British lowland rivers. In: Golosov, V., Belyaev, V., Walling, D.E. (Eds.), *Sediment Transfer through the Fluvial System. Proceedings of a Symposium Held in Moscow, August 2004*. IAHS Press 283, Wallingford, pp. 226–234.
- Williams, H., McBirney, A.R., 1979. *Vulcanology*, Freeman, Cooper and Co., San Francisco.
- Wolf, D., Baumgart, P., Meszner, S., Fülling, A., Haubold, F., Sahakyan, L., Meliksetian, Kh., Faust, D., 2016. Loess in Armenia—stratigraphic findings and palaeoenvironmental indications. *Proceedings of the Geologists' Association* 127, 29–39. <https://doi.org/10.1016/j.pgeola.2016.02.002>.
- Wright, V.P., 1989. Terrestrial stromatolites and laminar calcretes: a review. *Sedimentary Geology* 65, 1–13. [https://doi.org/10.1016/0037-0738\(89\)90002-X](https://doi.org/10.1016/0037-0738(89)90002-X).
- Wright, V.P., 2007. Calcrete. In: Nash, D.J., McLaren, S.J. (Eds.), *Geochemical Sediments and Landscapes*. Blackwell, Oxford, pp. 10–45.